Energy Reviews 4 (2025) 100118

Contents lists available at ScienceDirect

Energy Reviews

journal homepage: www.journals.elsevier.com/energy-reviews

Full Review Article

Emerging trends in electrochemical energy storage: A focus on low-temperature pseudocapacitors

Ziyang Zhu [a,c], Yu Liu [a,b,c,*], Hualiang Zhang [a,b,c], Yujie Xu [a,b,c], Zongping Shao [d], Lei Ge [e], Zhenbin Wang [f], Haisheng Chen [a,b,c,**]

[a] Energy Storage Research and Development Center, Institute of Engineering Thermophysics, Chinese Academy of Sciences, Beijing, 100190, PR China
[b] Nanjing Institute of Future Energy System, Institute of Engineering Thermophysics, Chinese Academy of Sciences, Nanjing, 211100, PR China
[c] University of Chinese Academy of Sciences, Beijing, 100190, PR China
[d] WA School of Mines: Minerals, Energy and Chemical Engineering, Curtin University, Perth, WA, 6845, Australia
[e] Centre for Future Materials, University of Southern Queensland, Springfield Central, QLD, 4300, Australia
[f] Department of Materials Science and Engineering, City University of Hong Kong, Hong Kong SAR, 999077, PR China

ARTICLE INFO

Keywords:
Supercapacitors
Low temperature
Electrodes
Electrolyte
Energy storage

ABSTRACT

Supercapacitors, also known as ultracapacitors or electrochemical capacitors, play a vital role in modern energy storage and electronic systems due to their outstanding characteristics. They boast high power density, making them ideal for applications requiring rapid energy delivery and absorption, such as electric vehicles for quick acceleration and regenerative braking. Additionally, their extended cycle life, enduring hundreds of thousands to millions of charge-discharge cycles, suits scenarios demanding consistent, long-term performance. The field of low-temperature pseudocapacitors (LTPCs) has seen significant advancements, becoming a key domain in energy storage research. This review explores the latest developments in LTPCs, highlighting their potential as efficient energy storage devices. It delves into their unique properties contributing to enhanced pseudocapacitive performance at low temperatures and dissects the electrochemical processes governing this phenomenon. Recent breakthroughs in device architectures and engineering strategies are showcased, addressing challenges like freezing-induced electrolyte degradation and reduced ion mobility. This review concludes by outlining potential research directions and key challenges for advancing LTPCs towards practical, widespread applications. It serves as a valuable resource for scientists, engineers, and policymakers, guiding the future development of energy storage technologies tailored for low-temperature environments.

1. Introduction

The escalating demand for energy storage solutions has prompted extensive research in electrochemical energy storage devices [1–5]. While conventional capacitors excel in high power density and rapid charge-discharge rates for applications requiring instantaneous bursts of energy, their limited energy storage capacity necessitates exploration of alternative technologies. Batteries offer higher energy density but are less suitable for scenarios requiring rapid energy delivery due to sluggish charge-discharge kinetics. This inherent trade-off has driven the quest for hybrid energy storage systems combining the strengths of capacitors and batteries. Pseudocapacitors, a category of electrochemical energy storage devices, leverage faradaic redox reactions at the electrode-electrolyte interface for charge storage and delivery [6]. Pseudocapacitive materials, known for reversible redox processes, bridge the gap between capacitive and battery-like behavior, revolutionizing energy storage. Notably, pseudocapacitors exhibit high performance at low temperatures, outperforming batteries due to the electrostatic nature of energy storage processes, short electrode separation, and absence of mass transport by diffusion [7–9]. In certain applications, such as in-space

* Corresponding author. Energy Storage Research and Development Center, Institute of Engineering Thermophysics, Chinese Academy of Sciences, Beijing, 100190, PR China.
** Corresponding author. Energy Storage Research and Development Center, Institute of Engineering Thermophysics, Chinese Academy of Sciences, Beijing, 100190, PR China.
E-mail addresses: liuyu@iet.cn (Y. Liu), chen_hs@iet.cn (H. Chen).

https://doi.org/10.1016/j.enrev.2024.100118
Received 20 June 2024; Received in revised form 5 August 2024; Accepted 16 October 2024

avionics, astronomical observatories, high-altitude aircraft, and polar region electrical systems, supercapacitors can replace batteries. The energy density of a supercapacitor is determined by its capacity (C) and the square of its potential window (V), as per the energy equation $E = 1/2CV^2$. The potential window and temperature tolerance of supercapacitors depend largely on electrolyte selection.

Depending on the solvents employed, electrolytes can be classified into organic, ionic liquid, and aqueous types. Organic electrolytes offer a wide electrochemical stability window (ESW), enabling organic supercapacitors to attain high cell voltages (ranging from 2.5 to 4.0 V), resulting in energy densities surpassing those of aqueous supercapacitors [10]. However, their extensive application faces challenges, including 1) a low ion diffusion rate due to relatively large ion size, 2) high production costs and the need for a meticulously moisture-free process, and 3) environmental pollution and safety concerns due to the presence of toxic and flammable components. Ionic liquids, often termed low-temperature molten salts, exhibit low vapor pressure, minimal volatility, excellent wettability, non-flammability, high thermal stability, and an expansive ESW of up to 6.0 V, indicating a promising outlook for their application in high-performance supercapacitors [11]. Nevertheless, they suffer from drawbacks such as low ionic conductivity and high viscosity, hindering ion transport and rate performance of supercapacitors. Additionally, they exhibit environmental sensitivity and come with a higher price tag. Aqueous electrolytes, known for high ionic conductivity, affordability, and eco-friendliness, hold significant potential in the supercapacitor field [12]. However, the decomposition voltage of water is limited to 1.23 V, significantly restricting cell voltage and impeding the progress of aqueous supercapacitors. Various strategies have been proposed to address this challenge, including adjusting the pH value of the aqueous electrolyte, modifying the potential of zero voltage of electrodes, balancing the mass of the two electrodes, and passivating the electrode surface. Despite these efforts, achieving cell voltages exceeding 2.0 V in aqueous electrolytes with expanded ESWs remains a formidable task.

Several studies have indicated the efficient operation of supercapacitors utilizing either aqueous or organic electrolytes even in extremely low temperatures, reaching as low as −40 °C [13,14]. This adaptability is ascribed to the heightened freezing point depression values induced by an increased ionic concentration. However, it is noteworthy that low-concentration aqueous-based electrolytes face a significant limitation at these extreme temperatures due to the risk of electrolyte freezing [15]. Aqueous electrolytes have gained substantial attention from a fundamental perspective, primarily due to their exceptional ionic conductivity, non-flammable nature, environmental friendliness, cost-effectiveness, and ease of handling, especially when compared to the organic electrolytes prevalent in most commercial devices. Regrettably, there exists a notable research gap concerning the physicochemical and electrical properties of highly concentrated aqueous-based electrolytes [16]. Electrolytes employing a multi-solvent system demonstrate commendable tolerance for low temperatures, attributed to the low viscosity and high dielectric constant of the organic solvent, in conjunction with the low-melting-point attributes of the organic co-solvent. For instance, when utilizing low-melting co-solvents like methyl formate (MF), methyl acetate (MA), ethyl acetate (EA) or 1, 3-dioxolane (DIOX), the practical operating temperatures of the assembled supercapacitor can decrease as low as −55 °C [17]. However, it is important to note that, even under such conditions, this specific supercapacitor achieves a working voltage window and specific energy density of only 2.3 V and 16 Wh kg^{-1} (based on the total mass of the two-electrode material) at −55 °C [18]. Another notable example involves a supercapacitor based on activated carbon, utilizing a 1 M $EMIMBF_4$/(AN + MA)-based electrolyte [19]. This system offers a high voltage window of 3.5 V and showcases a high energy density of 80 Wh kg^{-1} at a low temperature of −50 °C.

The diminished electrochemical performance of supercapacitor cells in low-temperature environments can be attributed to several key factors. Firstly, the high freezing point leads to reduced electrochemical performance at low temperatures. Secondly, reduced electronic conductivities of electrode materials at low temperatures result in slower reaction rates. Thirdly, weak compatibility between electrode materials and the electrolyte raises resistance levels and limits reaction rates. In response to these challenges, researchers have undertaken significant efforts to enhance the electrochemical properties of both electrode and electrolyte materials tailored for low-temperature supercapacitor cell applications. This comprehensive review meticulously examines the recent strides made in LTPCs, encompassing a diverse range of materials, architectural designs, and performance benchmarks. By drawing upon a substantial body of literature, we delve into the fundamental principles that underlie pseudocapacitive behavior, shedding light on the pivotal factors that govern the design and optimization of pseudocapacitor systems. This review aspires to offer a comprehensive panorama of the recent progress in LTPCs, delivering a thorough exploration of materials, architectural configurations, and performance indicators that define this rapidly advancing field.

2. Role and requirements of LTPCs components

The energy storage mechanism of pseudocapacitance involves intricate processes, including ion transmission and diffusion in electrolytes, interfaces, and electrodes, along with charge transfer at interfaces between electrolyte and electrodes. These processes encompass physical and Faraday processes, such as surface adsorption, solvation/desorption, ion insertion/extraction, and redox reactions [20]. However, at low temperatures, these processes are adversely affected, resulting in a decline in the electrochemical performance of LTPCs. This performance degradation includes the deterioration of ion accessibility and electron conductivity of the electrode, reduction in ion conductivity of the electrolyte, and deterioration of interfacial contact quality [21]. These challenges can be categorized into electrode-related and electrolyte-related issues, both intricately linked to the properties of the electrodes and electrolytes. To enhance the design of LTPCs, a comprehensive understanding of the mechanisms underlying electrode and electrolyte properties is crucial for maintaining high performance retention at low temperatures. This section introduces the key properties of electrodes and electrolytes critical for sustaining excellent low-temperature performance, examining their influencing factors, and presenting practical optimization strategies.

2.1. Electrode of LTPCs

Electrode materials, serving as a pivotal constituent of supercapacitors, wield a substantial influence on their overall performance. Properties like porous structure, high conductivity, and significant electrochemical activity are instrumental in facilitating the conduction, migration, and accumulation of electrons and ions, thereby determining the energy density of supercapacitors [22]. Despite these advantageous features, the degradation of certain electrode properties, particularly ion accessibility and conductivity, in low-temperature environments can result in inadequate performance. Therefore, to uphold optimal electrochemical functionality at low temperatures, electrodes must fulfill specific criteria: 1) possess a judicious pore structure ensuring efficient ion accessibility for streamlined ion transport; 2) exhibit high electrical conductivity to facilitate effective electron transport; and 3) demonstrate good compatibility to augment interface contact quality and overall electrochemical stability.

2.1.1. Proper porous structure

The nanoporous nature of electrodes confers several advantageous properties, including a shorter ionic diffusion distance and a larger surface area that exposes more active sites. These features are conducive to augmenting the energy density and power density of supercapacitors. In the context of supercapacitors operating under low temperatures, the importance of a porous structure in influencing electrochemical

performance becomes notably pronounced. Research indicates that a well-defined porous structure, characterized by attributes such as appropriate pore size, distribution, shape, and architecture, plays a crucial role in sustaining optimal supercapacitor performance at low temperatures [23–25].

Pores are typically classified into micropores (<2 nm), mesopores (2–50 nm), and macropores (>50 nm) based on their size. Micropores, characterized by smaller dimensions, exhibit a larger specific surface area, providing more sites for surface adsorption and electrochemical reactions, thereby promoting high energy density. However, micropores may have limited accessibility to larger ions, particularly in organic and ionic liquid electrolytes due to their larger size. This limitation results in a substantial reduction in capacitance during high-current charge/discharge conditions, and this capacitance decay is exacerbated at low temperatures due to sluggish ion diffusion, increased solvation energy, and slower desolvation processes (Fig. 1) [26,27]. In contrast, mesopores with larger sizes facilitate the direct entry of solvated ion clusters, offering improved ion accessibility that enhances ion diffusion from electrolyte to electrode and optimizes pore surface area utilization [28]. Consequently, electrodes with a higher proportion of mesopores have been observed to maintain robust capacity at low temperatures [29]. However, an increase in pore size may compromise specific surface area, potentially diminishing electrochemical performance. Therefore, judicious strategies are imperative for pore size regulation or the selection of appropriate electrolytes and salts, aligning pore dimensions with ion clusters to achieve concurrent high ion accessibility and a large specific surface area for the development of LTPCs with elevated energy density.

In addition to pore size, the distribution of pore sizes holds significant importance. Research indicates that mesoporous/microporous materials with a judicious distribution of micropores and mesopores demonstrate outstanding energy density and capacity retention at low temperatures [28]. Mesopores, characterized by larger pore volumes, serve as effective transport channels for ion diffusion, enhancing accessibility of ions to micropore surfaces. Additionally, the interconnected structure of micropores and mesopores mitigates the depth of micropores, preventing a reduction in energy density caused by ion entrapment [30]. Simultaneously, micropores contribute substantially to a large specific surface area, providing increased adsorption sites. The coexistence of mesopores and micropores with a well-balanced distribution offers favorable channels for ion diffusion and maximizes surface areas, thereby providing abundant active sites.

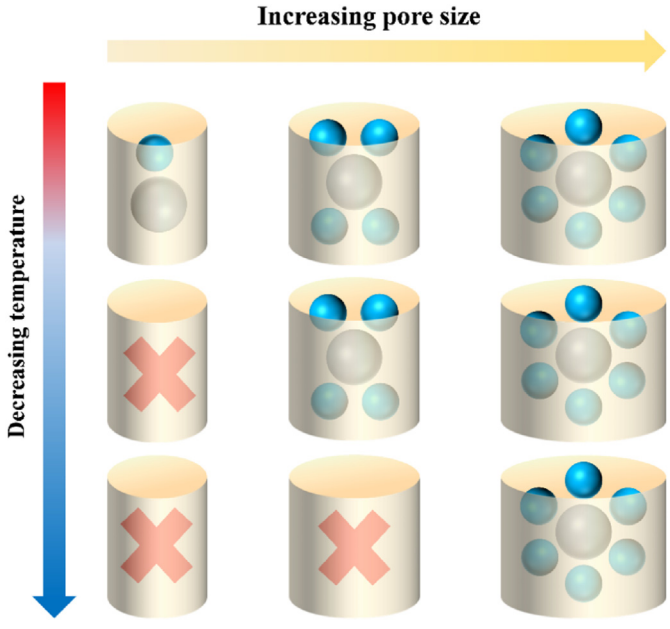

Fig. 1. The influence of temperature and pore size on the ion accessibility of pores. Reproduced with permission [26]. Copyright 2019, Elsevier.

Furthermore, the morphology of pores, including slit, cylinder, and sphere shapes, plays a crucial role in influencing ion accessibility. The structure of a slit pore confines a solvated ion in only one direction, with the smallest axis determining ion entry. In the case of cylinder-type pores, ions experience confinement in two directions, where the second largest axis limits their access. Sphere-type pores utilize their largest axis to confine solvated ions in all directions. Consequently, for pores of identical size, slit-type pores can accommodate solvated ions with the largest solvation number, effectively reducing the energy barrier that must be overcome [23].

The structural composition is another critical determinant of porous materials. Configurations featuring one-dimensional straight pores, two-dimensional layered spaces, or three-dimensional interconnected morphologies create unobstructed pathways for ion diffusion and serve as reservoirs for electrolyte ions. This construction effectively enhances the interfacial surface area and reduces the diffusion distance [24,25,28]. Consequently, several strategies have been devised to construct electrodes with a rational architecture for LTPCs, a topic that will be elaborated upon in subsequent sections.

2.1.2. High electronic conductivity

Materials demonstrating high electrical conductivity facilitate swift electron transfer within electrodes, minimizing energy losses and promoting efficient redox reactions, thereby enhancing rate capability. However, the electrical conductivity of materials is influenced by various factors, including crystal structure, porosity, and operating temperature. Among these factors, temperature is a critical variable affecting material conductivity. The temperature-dependent behavior of material conductivity is generally explained by two mechanisms: hopping transport and ballistic transport [31]. The distinction lies in the temperature dependence of their conductivities. In the case of hopping-type conduction, it is always thermally activated and follows an exponential law which can be expressed as

$$\sigma = \sigma_0 \, exp\left(-\left(\frac{T_0}{T}\right)^{\frac{1}{d}}\right) \tag{1}$$

where σ is the conductivity, T is the temperature, σ_0 and T_0 are the constants related to the material, and d represents the dimensionality of the sample. Consequently, higher temperatures lead to increased conductivity. Conversely, materials that conform to the ballistic transport mechanism may be either thermally activated or deactivated, depending on the carrier concentration of the material [32]. For materials with sufficiently high carrier concentration, such as metals, conductivity is limited by various scattering processes, which are enhanced by increasing temperature, resulting in reduced conductivity at higher temperatures. In contrast, for materials with insufficient charge carrier concentration such as semiconductors, their conductivity is limited by the charge carrier concentration. The charge carrier concentration in semiconductors increases with elevated temperature due to the generation of more electrons or holes at higher temperatures. Therefore, the conductivity of semiconductor materials follows the Arrhenius equation, $\sigma = \sigma_0 \exp(-E_a/kT)$, where E_a represents the activation energy associated with the band gap width, k is the Boltzmann constant. Many transition metal oxides commonly used in electrode active materials exhibit semiconducting properties, such as TiO_2, NiO, Fe_2O_3, and therefore exhibit poor electrical conductivity at low temperatures, limiting their applicability in extremely cold areas [33]. Consequently, when selecting electrode materials for LTPCs, it is crucial to consider their conductivity and temperature-dependent characteristics, giving preference to materials exhibiting high conductivity at low temperatures.

2.1.3. Compatibility

Adequate compatibility among electrode materials is imperative to

establish favorable interface contact, diminish interface internal resistance, and enhance the electrochemical performance of supercapacitors, particularly for LTPCs designed to operate across a broad temperature spectrum [34]. The disparate thermal expansion and contraction properties of distinct materials often result in insufficient interfacial contact between the electrode and the current collector, as well as within the components of the electrode material (active materials, adhesives, conductive additives) during significant temperature fluctuations. This phenomenon contributes to heightened interface contact resistance and suboptimal electrochemical performance [21,35].

Moreover, the compatibility between electrode materials and electrolyte significantly influences the ion transport, desolvation, and redox reactions at the interface, playing a pivotal role in the electrochemical stability of supercapacitors [36]. This compatibility involves both physical and chemical aspects. The physical aspect encompasses factors such as matching pore size with electrolyte ions, as discussed earlier. Additionally, wettability is a critical physical factor, denoting the liquid's spreading ability on a solid surface [37]. Electrodes with superior wettability promote the electrolyte's spread on the electrode surface and penetration into pores, effectively increasing the contact area and facilitating ion transport at the interface. The wetting of electrolyte on the electrode surface is influenced by various factors, including electrode surface properties (surfactant, roughness, etc.), temperature, and pressure. Temperature, among these factors, plays a prominent role in the entire system [38]. At higher temperatures, the contact angle typically decreases, indicating enhanced hydrophilicity of the electrode surface. This decrease results from the reduction of surface tension caused by the temperature increase. The diminished contact angle signifies increased interaction between the liquid and solid surface. Conversely, at lower temperatures, wettability diminishes, impeding ion transport at the interface and leading to suboptimal electrochemical performance. Consequently, optimizing wettability between electrodes and electrolytes is a crucial consideration in the design of LTPCs. Fortunately, researchers have devised effective strategies to enhance wettability, such as surface modification of electrode materials or the incorporation of additives into the electrolyte.

The chemical compatibility between the electrolyte and the electrode stands as a crucial determinant of the electrochemical stability in LTPCs. The electrochemical stability window, delineated by the upper and lower limits of electrolyte decomposition, is intricately linked to temperature-dependent redox reactions transpiring at the interface [36]. Notably, owing to the suppressed decomposition reaction of the electrolyte at lower temperatures, LTPCs typically manifest broader electrochemical windows during operation at reduced temperatures [39]. Consequently, despite the rate performance decline in LTPCs under low temperatures due to sluggish interfacial redox reaction kinetics, the extended electrochemical stability window facilitates the development of LTPCs with elevated energy density even in colder environments [39,40].

2.2. Electrolyte of LTPCs

Electrolytes, as pivotal components of LTPCs, wield substantial influence over electrochemical performance metrics such as power density, rate capacity, and safety. Attaining exemplary electrochemical performance necessitates electrolytes endowed with exceptional characteristics, including high ionic conductivity, thermal stability, and electrochemical resilience. However, certain electrolyte properties may undergo alterations at low temperatures, compromising LTPC performance. Factors such as diminished ionic conductivity, heightened viscosity, and slower desolvation contribute to elevated equivalent internal resistance and impaired rate capability at lower temperatures. Moreover, the risk of electrolyte freezing poses a significant threat, potentially resulting in device failure and safety hazards. Consequently, tailoring electrolyte properties to meet the requirements of low-temperature applications demands strategic optimization. A comprehensive understanding of temperature's impact on electrolytes is fundamental to designing formulations suitable for low-temperature environments. This section scrutinizes the effects of temperature on electrolytes, encompassing considerations related to melting points, ion conductivity, and essential factors guiding the design of low-temperature-resistant electrolytes.

2.2.1. Low freezing point

Electrolyte freezing constitutes a primary factor contributing to supercapacitor failure in low-temperature environments. Consequently, the imperative for progress in low-temperature supercapacitors hinges significantly on the development of electrolytes characterized by lower freezing points. A wealth of research endeavors has delved into the intricacies of electrolyte freezing mechanisms, yielding various practical strategies. Insight from these investigations reveals that the melting point of electrolytes is subject to diverse factors, encompassing environmental pressure, intermolecular forces, salt concentration, and other pertinent variables [40,41].

In adherence to the phase diagram of water (Fig. 2), within the Type I region, the melting point of ice undergoes a reduction to −22 °C as the pressure ascends to 207.5 MPa. This decrease in melting point concomitant with elevated pressure aligns with the principles elucidated by the Clapeyron equation:

$$\frac{dp}{dT}=\frac{L}{T\Delta V} \tag{2}$$

In the Clapeyron equation, where p represents the equilibrium pressure, T signifies the equilibrium temperature, L stands for the latent heat of the phase transformation, and ΔV denotes the volume change of the phase transformation process. Consequently, for water, during the phase transition from solid to liquid, the latent heat of the phase transition is positive, and the volume change is negative. Consequently, dp/dT is negative, implying that an increase in pressure results in a lower melting point. Nevertheless, the alteration in the freezing point of water with pressure is relatively marginal, especially when the pressure elevates from atmospheric pressure (0.1 MPa) to 1 MPa, a tenfold increase, leading to a change in melting point of less than 0.1 K. Consequently, attempting to reduce the melting point by augmenting pressure is not only intricate in execution but also economically inefficient.

The melting point of a solution is significantly influenced by intermolecular forces, wherein solvents with higher melting points generally exhibit stronger intermolecular attractions. Factors such as molecular mass, charge distribution or polarization, and charge density

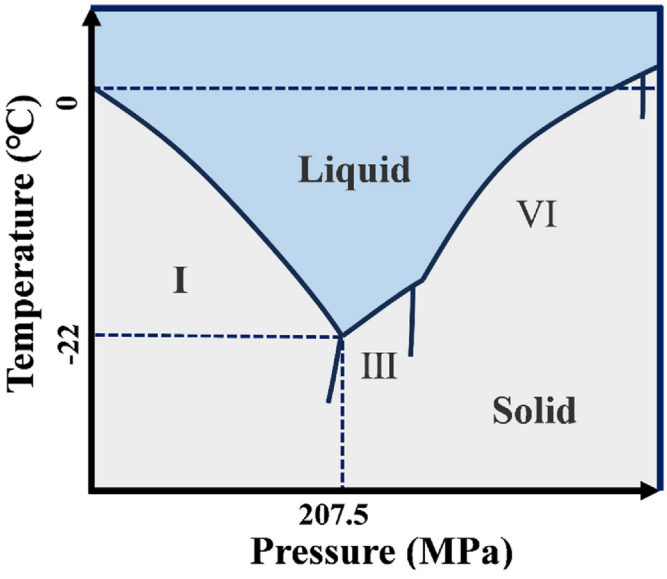

Fig. 2. The phase diagram of water.

concentration impact the intermolecular force. Solutions with larger molecular weights tend to have higher melting points due to increased van der Waals forces. However, water molecules, despite their relatively smaller molecular weight compared to H_2S, demonstrate a higher melting point due to the formation of hydrogen bonds. These bonds are a special type of strong intermolecular force present in compounds formed between hydrogen atoms and atoms with strong electronegativity, such as fluorine, oxygen, and nitrogen [42]. The freezing of water involves the formation of hydrogen bonds, driving the transformation from a disordered liquid to an ordered solid state [43]. This process begins with the formation of a compact ice nucleation, stabilized by a sufficient number of hydrogen bonds. The nucleation then undergoes changes in shape and size until reaching a stage conducive to rapid expansion, ultimately leading to the crystallization of the entire system [44]. The increase in hydrogen bonding during freezing transitions water from a liquid to a solid state. Recognizing the pivotal role of hydrogen bonds in the high melting point of aqueous solutions, various strategies have been developed to inhibit hydrogen bonding interactions between water molecules. These strategies aim to reduce the freezing point of aqueous electrolytes and include methods such as employing high-concentration salt solutions, adding antifreeze agents, and introducing gel networks [45,46].

Non-aqueous electrolytes, encompassing organic and ionic liquid electrolytes, generally feature lower freezing points (Table 1), rendering them promising for low-temperature applications. Nonetheless, they are not without limitations, with ion conductivity emerging as a crucial parameter influencing the performance of LTPCs [47].

2.2.2. High ionic conductivity

The ionic conductivity of an electrolyte stands as a critical determinant influencing the holistic performance of supercapacitors, encompassing aspects such as capacity, power density, rate capability, cycling stability, and safety [36]. Ionic conductivity (σ) is mathematically represented as the product of charge carrier (q), concentration (n), and mobility (b) [48]

$$\sigma = qnb \tag{3}$$

In liquids, the mobility can be associated with the viscosity (η) via Stokes equation [49]

$$\frac{b}{q} = \frac{1}{6\pi r\eta} \tag{4}$$

Where r is the effective radius of the ion. It is worth noting that the Stokes equation only agrees well in dilute solutions. The ionic conductivity of a solution is intricately influenced by the charge number, size, and concentration of the charge carriers, along with the viscosity of the electrolyte. Hence, when formulating a low-temperature supercapacitor electrolyte with a focus on achieving high ionic conductivity, careful consideration of the salt type and electrolyte viscosity becomes imperative.

Observing Equation (3), it becomes evident that the ionic conductivity of the electrolyte maintains a positive correlation with salt concentration. However, practical experiments reveal that as salt concentration increases, the ionic conductivity gradually reaches its zenith, and further increments result in a decline in ionic conductivity (Fig. 3). This phenomenon is attributed to the interplay of factors wherein, at low concentrations, heightened concentration augments carrier concentration, thereby enhancing conductivity. Simultaneously, the escalating concentration fosters increased anion-cation attraction, elevating viscosity and diminishing ion mobility, impeding ionic transport [50]. As concentration continues to rise, this hindrance progressively prevails, leading to the reduction in ionic conductivity at higher concentrations. Beyond the diminished conductivity associated with high concentration, the precipitation of salt at low temperatures emerges as a critical concern, limiting the operational temperature range. Fortunately, researchers have devised effective strategies to mitigate salt precipitation by modulating cation-cation interactions, such as incorporating cosolvents [50,51].

Viscosity, a force that resists fluid flow and obstructs the relative motion of solvent molecules in the electrolyte, directly hampers ion diffusion and serves as a measure of ion transport properties [52]. Research indicates that viscosity is subject to various influences, including temperature, salt type, and concentration. Generally, a decline in temperature and an escalation in concentration result in increased viscosity due to heightened interactions among particles (solvent molecules, anions, and cations). The magnitude of these interactions can be quantified using binding energy, establishing an exponential relationship between viscosity (η) and binding energy (E_b) as expressed by the following equation [53]:

$$\eta = A\ exp\left(-\frac{E_b}{\alpha k_B T}\right) \tag{5}$$

Where A is the pre-exponential fitting coefficient, α is the exponent fitting coefficient.

Therefore, constructing an electrolyte system with low binding energy is crucial for obtaining a low-viscosity electrolyte. This involves considering the forces between solvent molecules, the attraction among electrolyte ions, and the coordination between electrolyte molecules and

Table 1
The freezing point of solvents commonly used in supercapacitors.

Categorize	Solvent	Molecular Formula	Freezing point (°C)
Aqueous	Water	H_2O	0
Organic	Ethylene Carbonate	$C_3H_4O_3$	35–38
	Dimethyl Carbonate	$C_3H_6O_3$	2–4
	Ethylene Glycol	$C_2H_6O_2$	−13
	Ethyl Methyl Carbonate	$C_4H_8O_3$	−14.5
	1,3-Dioxane	$C_4H_8O_2$	−42
	Acetonitrile	C_3H_3CN	−45
	Propylene Carbonate	$C_4H_6O_3$	−49.2
	Acetone	C_3H_6O	−94.7
	Ethyl Alcohol	C_2H_5OH	−114.1
	Methanol	CH_3OH	−97.8
Ionic liquid	$EMIMBF_4$	–	15
	EMIMTFSI	–	4
	EMIMAc	–	−20
	$BMIMPF_6$	–	−10
	$BMIMBF_4$	–	−81

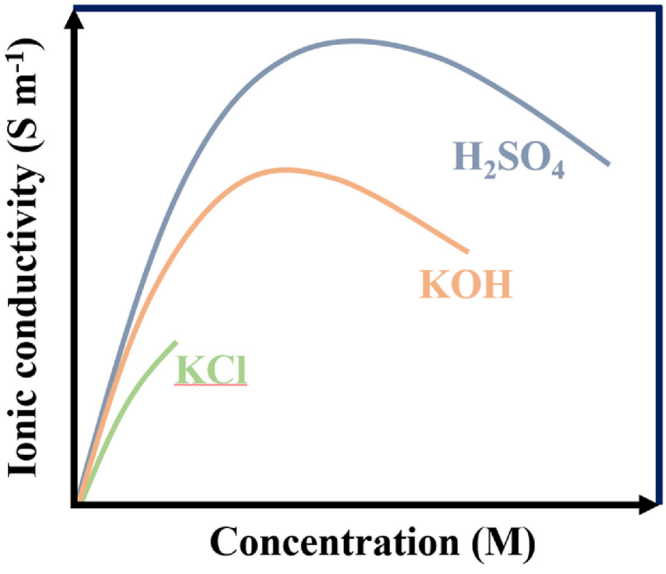

Fig. 3. The conductivity of KCl、KOH、H_2SO_4 electrolytes varies with concentration.

Table 2
Ionic radius, hydrated ionic radius, ionic mobility and molar ionic conductivity of the electrolyte ions in aqueous solution at 298 K [58–60].

Ion	Ionic radius (Å)	Radius of hydrated sphere (Å)	Ionic mobility (10^{-8} m^2 s^{-1} V^{-1})	Molar ionic conductivity (mS m^2 mol^{-1})
H^+	0.012	2.80	36.23	34.96
Li^+	0.59	3.82	4.01	3.87
Na^+	1.02	3.58	5.19	5.01
K^+	1.38	3.31	7.62	7.35
Zn^{2+}	0.74	4.30	5.47	5.28
OH^-	1.76	3.00	20.64	19.92
Cl^-	1.81	3.32	7.91	7.64
SO_4^{2-}	2.90	3.79	8.29	8.00

ions. Solvent molecules' interaction is primarily influenced by van der Waals forces, determined by molecular weight and polarity. Solvents with low molecular weight and low polarity may exhibit lower viscosity. However, it is noted that electrolytes with low viscosity often have lower dielectric constants according to empirical evidence [54]. The dielectric constant serves as a macroscopic representation of the electrolyte's microstructure, reflecting interactions between ions and molecules and influencing solvation patterns [55]. A high dielectric constant facilitates cation and anion solvation, promoting high ionic conductivity through strong ion-dipole interactions [56,57]. Conversely, non-polar solvents with low viscosity may exhibit low solubility to ionic compounds, hindering the increase of charge carrier concentration. Therefore, while pursuing low-viscosity solvents, it is essential to ensure adequate solvation ability to comprehensively optimize electrolyte properties.

As per equation (3), it becomes apparent that ion conductivity is affected not only by the viscosity and salt concentration of the solution but also by the charge number and radius of the solvated ions, contingent on the specific type of salt and solvent. Consequently, ions with smaller solvated sphere radii and larger charge numbers exhibit greater mobility, facilitating higher ion conductivity (Table 2) [58].

3. Strategies of developing LTPCs

According to the analysis presented in the second section, the electrode design for a low-temperature supercapacitor demands a precisely defined hierarchically interconnected porous structure with a rational distribution of pore size, shape, and distribution. This structure is essential for facilitating efficient ion transmission and maintaining high conductivity at low temperatures to support effective ion transport. Furthermore, electrodes must exhibit excellent compatibility with adjacent components to achieve optimal interface contact quality. The electrolyte, on the other hand, should demonstrate attributes such as a low melting point and high conductivity. This section delves into diverse and effective strategies for optimizing the design of electrodes, interfaces, and electrolytes.

3.1. Electrode optimization

3.1.1. Porosity modification

The optimization of the pore structure in electrodes is paramount for sustaining high-performance levels in LTPCs. Researchers have extensively explored reasonable pore structures that enhance ion accessibility and provide favorable ion transport channels. The regulation of pores necessitates precise control over their size, shape, and distribution. Achieving a rational pore architecture involves common strategies, including the judicious selection of synthesis methods, the utilization of nanomaterials with diverse dimensionalities, and the adoption of

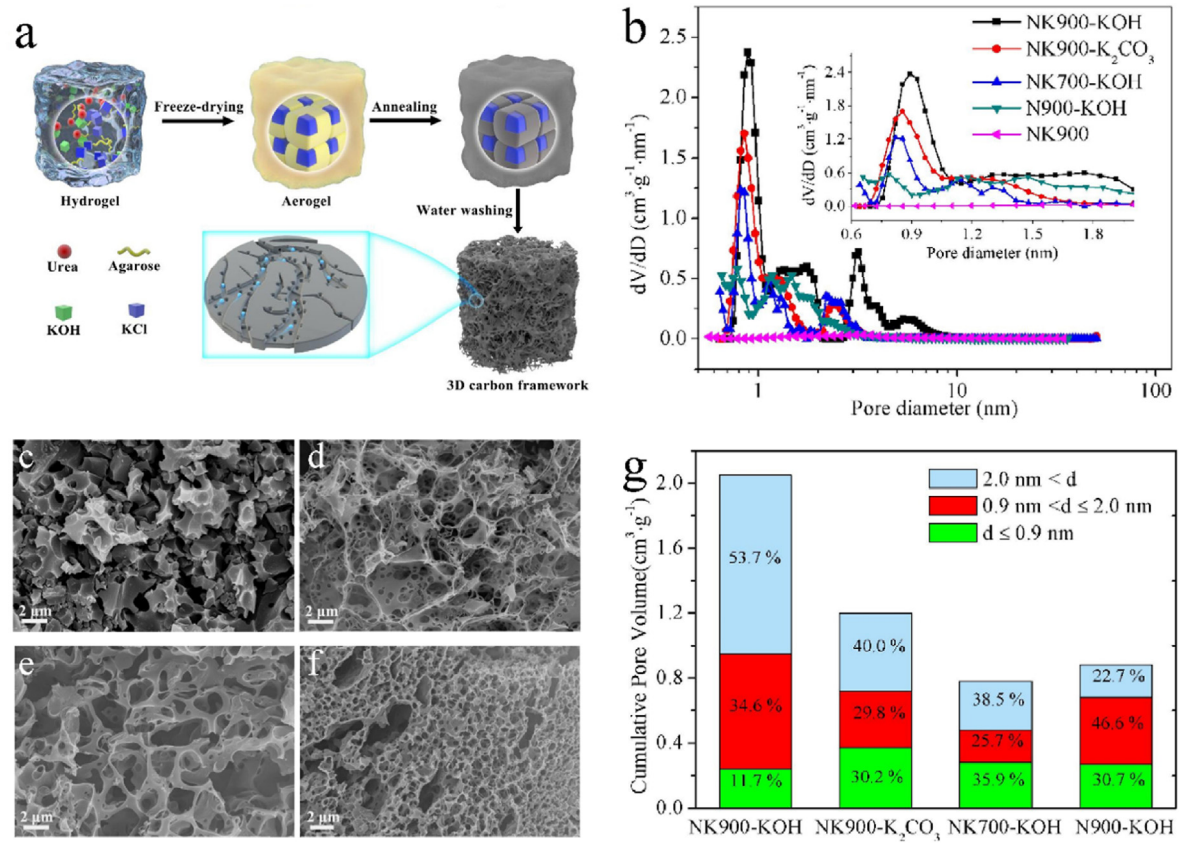

Fig. 4. (a) Schematic illustration for the preparation processes of the designed samples; (b) the corresponding pore size distributions; (c–f) SEM images of N900-KOH, NK900-KOH, NK700-KOH, and NK900-K_2CO_3; (g) pore volume ratio at different pore size range of the synthesized samples. Reproduced with permission [27]. Copyright 2022, Elsevier.

advanced manufacturing techniques.

Commonly utilized electrode materials for LTPCs include carbon materials and their derivatives, transition metal oxides, and conductive polymers. Carbon materials, owing to their porous properties and stability, are extensively employed as electrodes for supercapacitors or as substrates for loading other active substances. To achieve an ideal porous structure in carbon materials, researchers have undertaken extensive investigations, developing effective regulatory strategies such as the template method, aerogel method, polymer blending method, along with a judicious selection and preparation of specific precursors [24,27,29,61–63]. For instance, Pavlenko et al. [29] synthesized carbon materials with varying pore sizes using the template method to elucidate the importance of mesopores for the low-temperature performance of supercapacitors. The porous carbon samples, denoted as "SGT12nm" and "SGT8nm," were synthesized using d-Glucose as the carbon source and colloidal silica suspensions with particle sizes of 12 nm and 8 nm as hard templates, respectively. Subsequent pyrolysis and leaching processes were employed to eliminate the silica templates. The study demonstrated the feasibility of using silicon dioxide templates with different particle sizes for the regulation of pore size. In another study, Liu et al. [27] employed a one-pot strategy with potassium salt as a template and pore-forming agent to synthesis porous carbon. The preparation procedure is presented in Fig. 4a. Aerogels were formed through a series of processes including dissolution, stirring, cooling, and lyophilization using agarose, potassium salt, and urea as precursors. The precursor was then carbonized and washed to form a porous carbon sample. Different samples, denoted as NK900-KOH, NK900-K_2CO_3, N900-KOH, NK900, and NK1000-KOH, were synthesized by varying parameters such as carbonization temperature, chemical activator, and the addition of KCl. Consequently, the samples with KCl as a salt template exhibit a large number of micron cavities (Fig. 4d, e and f), which can act as ion-buffering reservoirs, contributing to the rate performance, while N900-KOH shows a broken bulk-like structure (Fig. 4c). NK900-KOH possesses mesopores ranging from 3 to 8 nm and micropores ranging from 0.9 to 2.0 nm (Fig. 4b), displaying the highest specific surface area and pore volume (Fig. 4g). Compared to NK900-KOH, NK700-KOH exhibits reduced pore generation (Fig. 4e) due to the suppressed reaction of KOH with carbon at a lower temperature, NK900-K_2CO_3 presents a

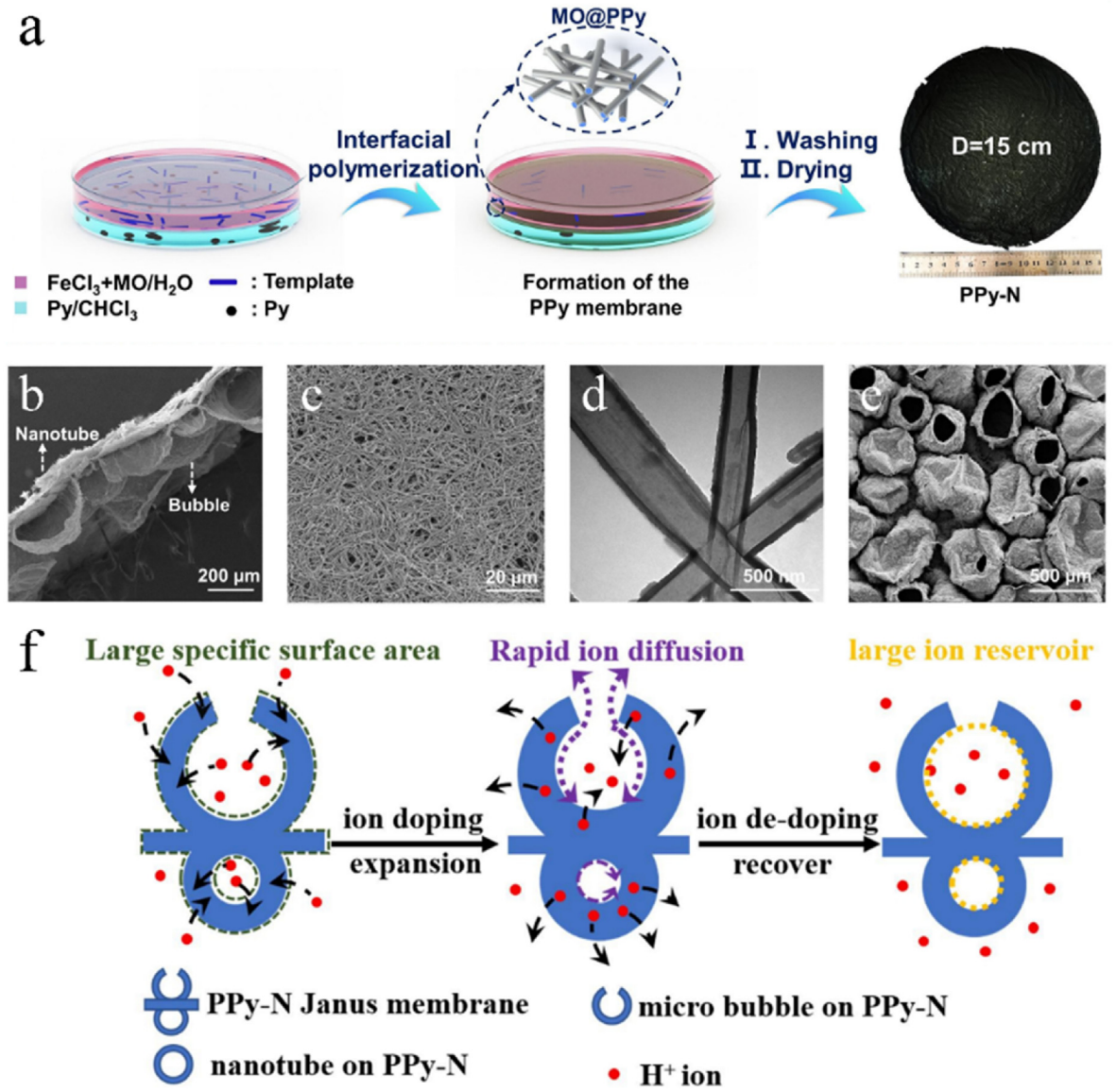

Fig. 5. (a) Schematic diagram of the synthetic method of PPy-N; (b–e) morphology of PPy-N: (b) SEM image of the cross-section, (c) SEM image of the nanotubes, (d) TEM image of the nanotubes, (e) SEM image of the bubbles; (f) schematic diagram of PPy-N energy storage mechanism. Reproduced with permission [64]. Copyright 2021, Elsevier.

smaller number of connect channels on carbon frameworks (Fig. 4f) due to the less activation capacity of K_2CO_3 compared to KOH. With a large number of micron cavities and connect channels on carbon frameworks, NK900-KOH demonstrated the best rate performance at a low temperature of −40 °C due to its higher mesoporous content facilitating ion diffusion.

Similarly, transition metal oxides possessing mesoporous pores exhibit a high specific surface area and a suitable pore size distribution. These characteristics facilitate effective contact between the electrolyte and electrode, enabling the rapid transfer of ions and charges at the interface, thereby demonstrating outstanding electrochemical performance [65,66]. Researchers have devised numerous effective strategies, including the hydrothermal method, template method, template-free method, microwave-assisted heating method, sol-gel method, etc., to obtain transition metal oxides with a porous structure [67–69]. However, their direct application at low temperatures is hindered by poor conductivity, particularly in combination with highly conductive materials.

Conductive polymers, known for their ability to maintain robust conductivity at low temperatures, exhibit significant potential for applications in low-temperature supercapacitors [70]. In a pioneering study, Zhang et al. [64] employed template-assisted polymerization to synthesize a polypyrrole electrode featuring a hierarchical structure, representing the first-known low-temperature-resistant electrode composed of a conductive polymer (Fig. 5a). The polypyrrole membrane electrode displayed a distinctive hierarchical arrangement, with nanotubes of 300 nm diameter and approximately 30 nm thickness cross-linked on one side, generating micropores (Fig. 5b, c and d). On the other side, microbubbles with a diameter and thickness of 300–500 μm and 200 nm, respectively, were present (Fig. 5e). The large pore size not only facilitated a high volume of electrolyte absorption, thereby reducing the ion diffusion distance, but also endowed the electrode with the ability to withstand repeated expansion and strain relaxation during charging and discharging cycles, ensuring superior structural stability. Furthermore, the presence of nanotubes and generated micropores contributed to an increased specific surface area of the electrode (Fig. 5f). Consequently, this electrode demonstrated notable flexibility and outstanding electrochemical performance even at an extremely low temperature of −50 °C.

In addition to optimizing the synthesis methods of materials, employing nanomaterials with diverse dimensions has proven to be an effective strategy for constructing rational pore structures. Nanomaterials find extensive use in electrode material research owing to their substantial specific surface area and increased active sites. These nanomaterials can be categorized based on dimensionality into zero-dimensional (0D), one-dimensional (1D), two-dimensional (2D), and three-dimensional (3D) nanomaterials [71]. 0D materials encompass small particles such as atomic clusters, nanoparticles, and quantum dots, exhibiting high specific surface area and stability. Furthermore, nano-scale particles significantly elevate the surface reaction rate, leading to a notable increase in power density [72]. Consequently, various transition metal oxide particles, including Fe_2O_3 [73] and RuO_2 [74], are employed to enhance supercapacitor capacity. However, due to their substantial surface energy, these particles are prone to aggregation, resulting in compromised rate capacity and cycle instability [75]. To address this challenge, 0D materials are often strategically loaded onto other materials to prevent aggregation.

1D materials, such as nanorods, nanotubes, and nanowires, possess a large aspect ratio and relatively high surface area, providing effective ion diffusion channels and shortening the distance of ion diffusion. These characteristics render them suitable for LTPCs with stringent requirements for ion accessibility. In a study conducted by Wei et al. [76], a 1D $Ni(OH)_2$ nanorod bundle, composed of finer nanorods with a diameter of approximately 16 nm, was utilized as an electrode for LTPCs. Comparative analysis revealed that the 1D nanorod bundle exhibited a 1.6-fold enhancement in performance under corresponding scan rates and current densities compared to 2D $Ni(OH)_2$ nanosheets. This improvement can be attributed to the nano-scale transport distances provided by the 1D nanorods for OH- ions and electrons, facilitating their conduction. Additionally, the larger contact area between the electrode and electrolyte enhances the utilization efficiency of the active material $Ni(OH)_2$. Moreover, the unique bundled structure of $Ni(OH)_2$ nanorods offers abundant interaction points among fine nanorods, restraining their movement while allowing sufficient deformation space to maintain both stability and ion accessibility simultaneously. When combined with binary solute electrolytes to form supercapacitors, these electrodes demonstrated an excellent specific capacitance of 332.4 F g^{-1} at 0.5 A g^{-1}, rate capability, and long cycling life, with 90.21 % capacitance retention after 10 000 cycles at 5 A g^{-1}, even at −30 °C.

2D materials, such as graphene and MXene, exhibit substantial specific surface areas and nearly resistance-free ion diffusion layers, making them highly suitable for LTPCs [77–79]. As an illustrative example, Chang et al. [80] employed the layered metal phosphide InP3 as the electrode material. The 2D structure of InP_3 provides a larger specific surface area and numerous active sites. Additionally, InP_3 nanosheets, obtained through liquid phase exfoliation technology, feature a porous structure conducive to electrode-electrolyte contact, providing ion diffusion channels and shortening ion diffusion distances. Due to its high conductivity, this electrode demonstrates exceptional performance across a broad temperature range, from −25 °C to 70 °C. However, 2D nanomaterials with a layered morphology are susceptible to irreversible stacking phenomena, leading to a reduction in effective surface area [81–83]. To counteract this stacking phenomenon, it is necessary to employ various strategies to regulate interlayer space, such as heteroatom doping, chemical activation, and composite materials [39,84–86]. For instance, Xu et al. [9] achieved $Ti_3C_2T_x$ sheets with only one or two layers by subjecting Ti_3AlC_2 to ultrasonic treatment after synthesizing $Ti_3C_2T_x$ powder through etching. This process ensures the entrapment of water molecules between the layers of $Ti_3C_2T_x$, providing an efficient transport pathway for ions to migrate towards functional groups. Furthermore, a comparative analysis of wet and dry MXene electrodes using concentrated sulfuric acid electrolyte at −70 °C demonstrated the exceptional rate capability of wet MXene electrodes. Even at −60 °C and a scan rate of 5 mV s^{-1}, cyclic voltammetry (CV) curves remained nearly identical to those observed at room temperature, with only a slight reduction in area. At −50 °C and a scan rate of 200 mV s^{-1}, wet MXene electrodes retained their CV curve shape. In contrast, dry MXene electrodes displayed a significant decrease in the CV curve at low scan rates (5 mV s^{-1}) due to higher internal resistance (150 Ohms at −50 °C) compared to wet MXene electrodes (4 Ohms). These findings underscore the immense potential of pre-intercalated MXene electrodes for applications requiring low temperatures.

3D materials encompass a diverse array of microstructures, including core-shell structures, hollow structures, and flower-like structures, among others. Distinct from 0D, 1D, and 2D nanomaterials, the 3D porous structure, in addition to its high specific surface area, possesses the capability to accommodate electrolyte, facilitate ion diffusion, and augment the contact area, thereby providing more accessible active sites [75,87]. These inherent properties underscore the potential applications of 3D materials in low-temperature environments. Such materials may consist of 0D, 1D, and 2D components or be synthesized using specific methods [88,89]. For example, Qin et al. [90] employed a nitrogen-doped three-dimensional porous graphene and carbon nanotube mixed film as the substrate for the growth of Ni-doped MnO_2, resulting in the fabrication of a composite electrode denoted as N-3DG/CNTs@Ni-MnO_2. The porous graphene with a 3D structure, synthesized by chemical vapor deposition, effectively mitigates the restacking problem associated with 2D graphene layers, which can lead to inadequate electrochemical performance, especially at low temperatures [91]. To enhance the low volume energy density of 3D graphene, carbon nanotubes and inorganic active materials are introduced. Consequently, the synthesized N-3DG/CNTs@Ni-MnO_2 composite electrode exhibits an interconnected porous structure that facilitates

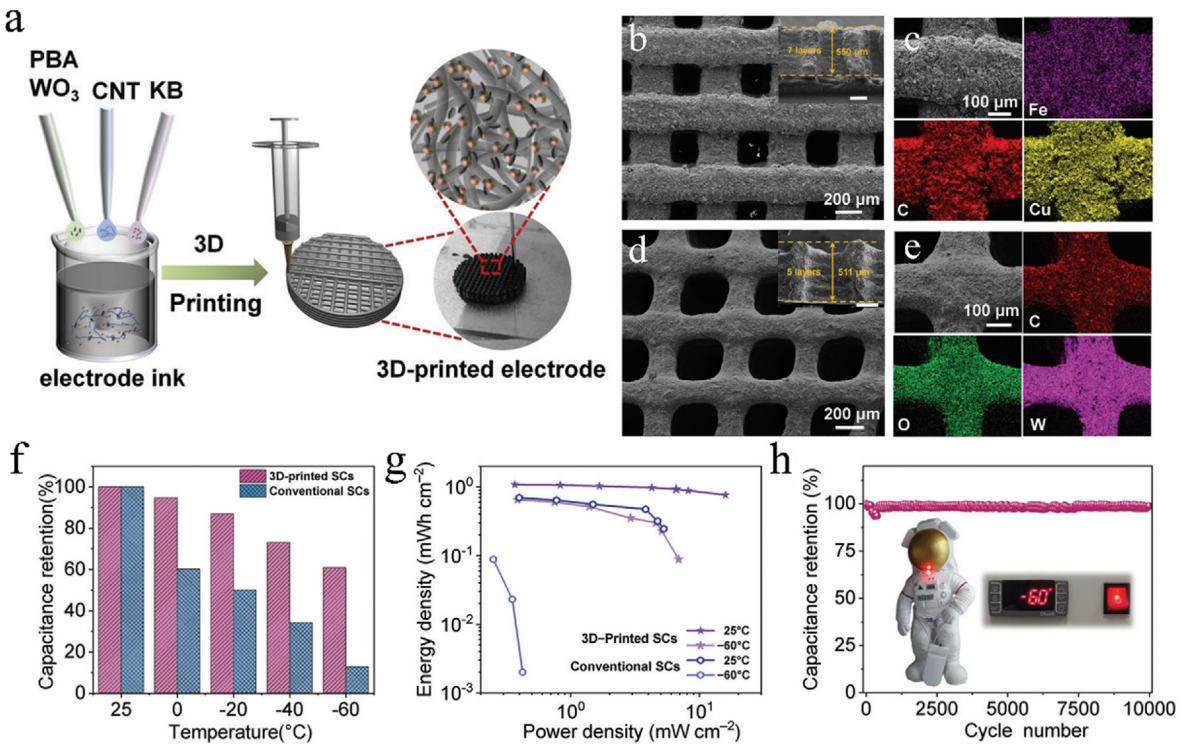

Fig. 6. (a) Schematic diagram showing the preparation process of the 3D-printed electrode with inks; (b, d) Top-view SEM images of the 3D-printed PBA/KB/CNT electrode (b) and the 3D-printed WO_3/KB/CNT electrode (d); (c, e) SEM images of the connected filament and corresponding elemental mapping of the 3D-printed PBA/KB/CNT electrode (c) and the 3D-printed WO_3/KB/CNT electrode (e); (f) The capacitance retention of SCs at different temperatures; (g) Ragone plot of 3D-printed SCs and conventional SCs at different temperatures; (h) Cycling performance of 3D printed SCs at −60 °C. Reproduced with permission [92]. Copyright 2023, Wiley-VCH.

ion/electron transport, demonstrating a high energy density of 78.88 mWh cm^{-3} and a volumetric capacitance of 46.4 F cm^{-3} at a scan rate of 30 mV s^{-1} under low-temperature conditions of −20 °C.

The advancement of sophisticated manufacturing techniques has introduced novel strategies for pore optimization, such as 3D printing and laser technologies. In recent years, the continual progress in 3D and 4D printing technology has revealed significant potential for achieving precise structural designs, rendering it particularly suitable for applications in low-temperature supercapacitors that require meticulous pore structure design. For instance, Zhang et al. [92] employed a direct ink writing technique to fabricate a low-temperature WO_3 electrode with a 3D structure. The preparation process of the 3D-printed electrode is presented in Fig. 6a. The 3D printed electrodes features a distinctive interconnected porous structure, which consist of cylindrical rods (Fig. 6b and d), facilitating electrolyte penetration and ion diffusion. In addition, the homogeneous distribution of elements on the electrode (Fig. 6c and e) shows that the 3D printed electrode achieves good compatibility and mixability. Consequently, the resulting 3D-printed supercapacitors show better capacity retention and electrochemical performance at low temperatures than conventional supercapacitors, retaining over 61 % of room temperature capacitance even at extremely low temperatures of −60 °C (Fig. 6f, g and h). Li et al. [93] utilized 4D printing technology to achieve tailored fabrication of MXene hydrogels, resulting in the formation of MXene hydrogels with a 3D porous structure, elevated specific surface area, and enhanced conductivity. These hydrogels demonstrated efficient pseudocapacitive energy storage capabilities, making them highly suitable for LTPCs.

3.1.2. Doping

Heteroatom doping emerges as a potent strategy for the modulation of various material properties, encompassing conductivity, wettability, and redox activity. Consequently, it has become a widely employed approach for the optimization of electrode materials, spanning carbon-based electrodes, transition metal oxide-based electrodes, and conductive polymer-based electrodes in the context of LTPCs [25,94–96].

Carbon-based materials, including porous carbon, carbon nanotubes, and graphene, are extensively employed in the development of low-temperature supercapacitors due to their remarkable conductivity, stability, and high specific surface area. However, owing to the energy storage mechanism of double-layer capacitors, carbon materials often exhibit higher power density but lower energy density compared to pseudocapacitors [97–100]. Fortunately, the introduction of heteroatoms, such as B, N, O, P, S, through doping offers an avenue to enhance the energy density of carbon materials by introducing additional active functional groups [25,95,96,100–102]. For example, Zhang et al. [103] synthesized a three-dimensional nitrogen-doped carbon framework using potassium citrate as the carbon precursor and activator, with anion exchange resin serving as both the carbon precursor and nitrogen source. This material exhibited a layered porous structure with a significantly large specific surface area of 1265.6 m^2 g^{-1}. The incorporation of O-/N-containing functional groups provided pseudocapacitance, contributing approximately 29 % to its total specific capacitance. When combined with a PVA-based electrolyte, the assembled supercapacitor achieved an impressive energy density of 17.4 Wh kg^{-1} at −20 °C. Similarly, Liu et al. [27] introduced urea during the one-pot synthesis of porous activated carbon, resulting in nitrogen-doped carbon materials with increased surface area. The heteroatom doping altered the surface polarity, enhanced hydrophilicity, and improved the interfacial interaction between the electrolyte and electrode, increasing the accessible surface areas of ions. Moreover, compared to single atom doping, multi-atom-doped carbon materials exhibit superior properties [104,105]. Sun et al. [106] synthesized N/S co-doped hierarchical porous carbon (N/S-HPC) using a versatile precursor of protic ionic liquids ([Megl][HSO_4]). The introduction of N, S, and O atoms into the carbon

framework enhanced conductivity, improved surface wettability, and provided additional pseudocapacitance. The material exhibited a high specific capacitance of 347 F g^{-1} at a current density of 0.5 A g^{-1}, demonstrating excellent cycling stability even after 5000 cycles in a 6 M KOH solution, while maintaining these properties at a low temperature of −20 °C.

Doping is a widely employed strategy for optimizing transition metal oxide/hydroxide materials [107,108]. Transition metal oxides, exemplified by RuO_2 and IrO_2, demonstrate notable specific capacitance, excellent conductivity, and superior power density and energy density. However, their high cost and toxic properties limit widespread application [109]. In contrast, alternative transition metal oxides like MnO_2, TiO_2, Co_3O_4, NiO, and $Ni(OH)_2$ are promising due to their high theoretical capacity, cost-effectiveness, and environmental friendliness. Despite these advantages, their inherent low conductivity poses challenges in achieving high theoretical energy density, especially in low-temperature environments where ion and electron transport face hindrances [25,102,110–112]. Oxygen vacancies have been identified as crucial for charge conduction in transition metal oxides [113]. Therefore, various doping methods, including in-situ metal ion self-doping strategies such as thermal annealing in an oxygen-deficient environment, hydrogen gas treatment, wet chemical reduction, electrochemical reduction, as well as heteroatom and dual-ion doping strategies, have proven effective in enhancing the conductivity of transition metal oxides through the introduction of oxygen vacancies [114–117]. For instance, Wu et al. [118] synthesized oxygen vacancy-enriched MoO_{3-x} nanobelts by incorporating ethyl alcohol into the hydrothermal synthesis of MoO_3. Ethyl alcohol played a crucial role in reducing Mo^{6+} to Mo^{5+} or Mo^{4+} during the synthesis process. This reduction of Mo^{6+} from the interior to the exterior of the synthesized nanobelts generated numerous oxygen vacancies, acting as shallow donors that increased charge carrier concentration. This enhancement improved electrode conductivity and reaction kinetics in the bulk. Consequently, these oxygen vacancy-enriched MoO_{3-x} nanobelts exhibited superior electronic conductivity, showcasing excellent electrochemical properties even at low temperatures.

In addition to influencing oxygen vacancies, the doping of foreign atoms can finely adjust the band gap and introduce additional reversible redox reactions, thereby enhancing conductivity and capacity. Guan et al. [119] successfully synthesized a novel electrode material, C, N, and Ag-doped layered nickel-cobalt-manganese ternary hydroxide (C/N-CNMA), addressing the issues of poor stability and electrical conductivity in nickel-cobalt-based double hydroxides at low temperatures. Experimental results demonstrated that C/N-CNMA exhibited higher conductivity, improved stability, and enhanced specific capacity due to the doping of manganese and silver elements. Characterization results revealed that the manganese-doped C/N-CNM exhibited a typical layered structure, effectively increasing the specific surface area and providing more active sites for charge-discharge reactions. The introduction of silver into C/N-CNMA resulted in a hollow structure formed by densely stacked nanosheets, creating numerous channels and exposing more active sites. However, further introduction of silver led to the appearance of amorphous structures in the material, causing a decrease in specific surface area compared to C/N-CNM. Despite the lower specific surface area, C/N-CNMA exhibited more significant battery-type charge-discharge characteristics and superior electrochemical performance than C/N-CNM. Density functional theory calculations revealed that the introduction of silver atoms induced noticeable deformation in the metal-oxygen chemical bonds and the structure of C/N-CNMA. The decrease in XRD pattern diffraction peak intensity indicated reduced crystallinity due to lattice distortion caused by the mismatch between the radius of silver atoms and that of Ni, Co, Mn atoms. Furthermore, the calculations showed that the doping of Mn atoms reduced the energy band of C/N-CNM, and the doping of Ag atoms further lowered the energy band of C/N-CNMA, resulting in higher conductivity. Moreover, it was observed that amorphous or low-crystallinity structures possess better adsorption properties for OH* and O*, making them more reactive with electrolyte ions during the charging and discharging process. Consequently, the C/N-CNMA materials obtained by doping manganese and silver atoms exhibited both high activity and stability, maintaining superior adsorption characteristics even at an ambient temperature as low as −35 °C compared with C/N-CNM and C/N-CN.

Substituting oxygen with anions, such as carbon, nitrogen, sulfur, and phosphorus, has proven to be an effective strategy for modulating the electrical conductivity of materials [120–122]. Transition metal phosphates, including InP_3, CoP, and CoP_3, exhibit higher conductivity and specific capacity compared to transition metal oxides, attributed to the multiple valence states and metal-like properties of phosphorus. This phenomenon has been observed in various studies [80,123,124]. Beyond transition metal phosphides, other materials like transition metal carbides, transition metal nitrides, and transition metal sulfides, such as MXene, M − MoS_2, and TiC, demonstrate significant potential for application in low-temperature supercapacitors due to their excellent conductivity and stability [9,122,125].

Doping strategies are extensively employed to enhance the low-temperature properties of conductive polymers. Studies indicate that the conductivity of conductive polymers can be effectively modulated by employing various dopants or adjusting doping levels, spanning a wide range from 10^{-10} to 10^{4} S cm^{-1} [126].

3.1.3. Composite materials

Carbon-based materials, transition metal oxides, and conductive polymers, among other materials commonly employed in LTPCs, each present distinct advantages and limitations. Achieving high-performance LTPCs using a single material type is challenging due to these inherent characteristics. For example, carbon materials offer high porosity, conductivity, and stability, rendering them suitable for supercapacitors operating at low temperatures. However, their electric double-layer energy storage mechanism often results in relatively low capacity. On the other hand, transition metal oxides exhibit high capacity but suffer from poor conductivity, while conductive polymers, though possessing adequate conductivity, may exhibit lower stability. Thus, there is a compelling need to integrate the strengths of various material types to create composite materials that demonstrate exceptional overall performance.

Carbon-based materials are frequently employed as substrates for incorporating transition metal oxides, leveraging their exceptional porosity, electrical conductivity, and stability. This integration enhances the overall conductivity and stability, particularly in low-temperature environments [127]. For instance, Sun et al. [84] conducted the synthesis of a novel composite material, denoted as Mn_3O_4-embedded 3D N/P co-doped carbon cloth/carbon foam (Mn_3O_4-NPCN/CF), utilizing a high-temperature pyrolysis method. The composite exhibited a 3D interconnected carbon framework that facilitated ion transport, ensuring outstanding stability and conductivity. The embedded Mn_3O_4 contributed additional pseudocapacitance for charge storage. Furthermore, the introduction of N and P atoms enhanced both electrode surface wettability and the voltage window, resulting in improved electrochemical performance. This composite strategy effectively combined the porous structure of the doped carbon material, which facilitates ion transport, with the high charge capacity provided by Mn_3O_4, addressing challenges such as poor electrical conductivity (10^{-5} - 10^{-6} S cm^{-1}), limited cycling stability, and the small wetting surface of Mn_3O_4. Through their synergistic effects, the composed electrode exhibited excellent performance at low temperatures. Similarly, Kong et al. [128] designed a well-aligned hierarchical pseudocapacitive electrode composed of graphene nanosheets and MnO_2 nanosheets (Fig. 7a). The fabrication process of GN/VGNS/MnO_2 is presented in Fig. 7b. It featured run-through channels formed by graphene networks (GN) as ion-buffering reservoirs

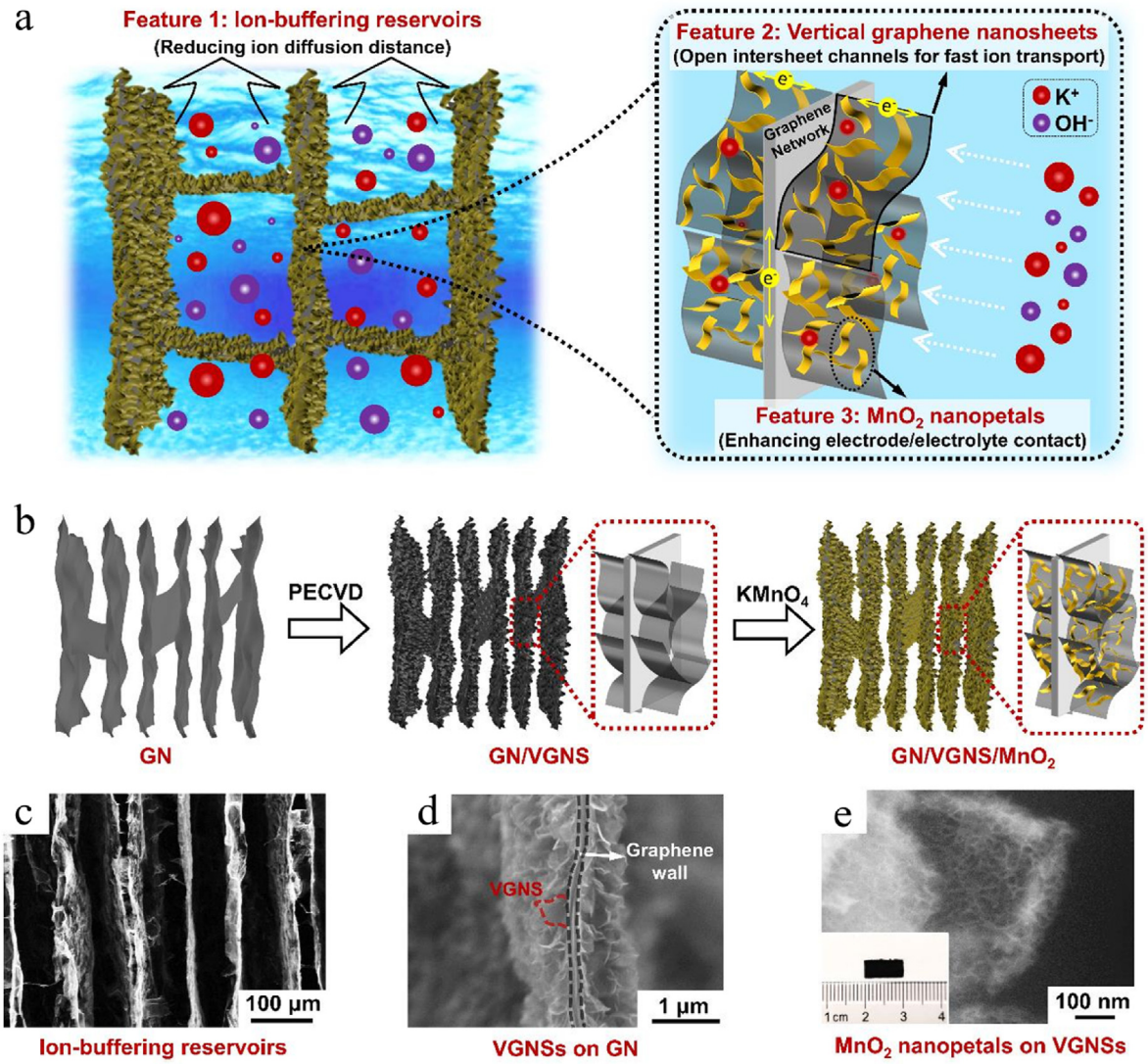

Fig. 7. Schematic illustration of (a) the hierarchical GN/VGNS/MnO_2 structure and its features and (b) the fabrication process of GN/VGNS/MnO_2; Cross-sectional SEM images of (c) GN and (d) VGNSs grown on an individual graphene wall in the GN; The representative VGNS and graphene wall in (d) are outlined with red and black dash lines, respectively. (e) A close-up of MnO_2 nanopetals grown on VGNSs; The inset in (e) shows an optical image of the GN/VGNS/MnO_2 sample. Reproduced with permission [128]. Copyright 2019, Wiley-VCH.

(Fig. 7c), open inter-sheet channels between vertical graphene nanosheets (VGNS) for fast ion transport (Fig. 7d), and enhanced interfacial contact for efficient pseudocapacitive reactions of MnO_2 (Fig. 7e). Under the synergistic effect of these characteristics, the electrode exhibited a shortened ion diffusion distance, fast ion diffusion, and enhanced interface pseudocapacitive reactions. Consequently, the pseudocapacitive electrode-based device demonstrated excellent capacity retention at low temperatures, maintaining 90.7 % and 80.8 % of room-temperature capacitance at 0 °C and −30 °C, respectively. In summary, this study produced a pseudocapacitor with outstanding temperature stability, comparable to electric double-layer capacitors, by combining graphene nanosheets with MnO_2 nanopetals and implementing reasonable structural design.

In addition to serving as a substrate for transition metal oxides, carbon-based materials can be amalgamated with conductive polymers to create composite materials, compensating for their individual limitations [129,130]. For instance, Guo et al. [131] engineered a fiber supercapacitor employing a composite material comprising carbon nanotubes and polypyrrole (PPy). Carbon nanotubes, characterized by a unique one-dimensional structure, excellent electrical and mechanical properties, and chemical stability, possess high capacity but are limited by the electric double-layer energy storage mechanism and a restricted effective surface area. On the other hand, PPy, known for its flexibility and high capacity due to the pseudocapacitance mechanism, suffers from poor mechanical properties. The authors utilized carbon nanotubes as the framework and coated them with conductive polymer PPy to produce composite materials exhibiting both high capacity and superior mechanical properties, coupled with flexibility. The assembled fiber supercapacitor, based on these composite materials, demonstrated high stability and reliability, functioning efficiently at a low temperature of −27 °C. Similarly, graphene can be employed to enhance the mechanical properties of PPy. However, the introduction of graphene typically diminishes the crystallinity of PPy, resulting in suboptimal electrochemical performance [132]. Addressing this challenge, Wu et al. [132] synthesized a nanocomposite material comprising graphene-silver-polypyrrole. While PPy contributes pseudocapacitance and maintains good conductivity at low temperatures, it exhibits poor stability. The incorporation of graphene effectively enhanced the flexibility and mechanical properties of PPy but reduced its crystallinity. Fortunately, the introduction of silver nanoparticles significantly increased the crystallinity of PPy over a wide

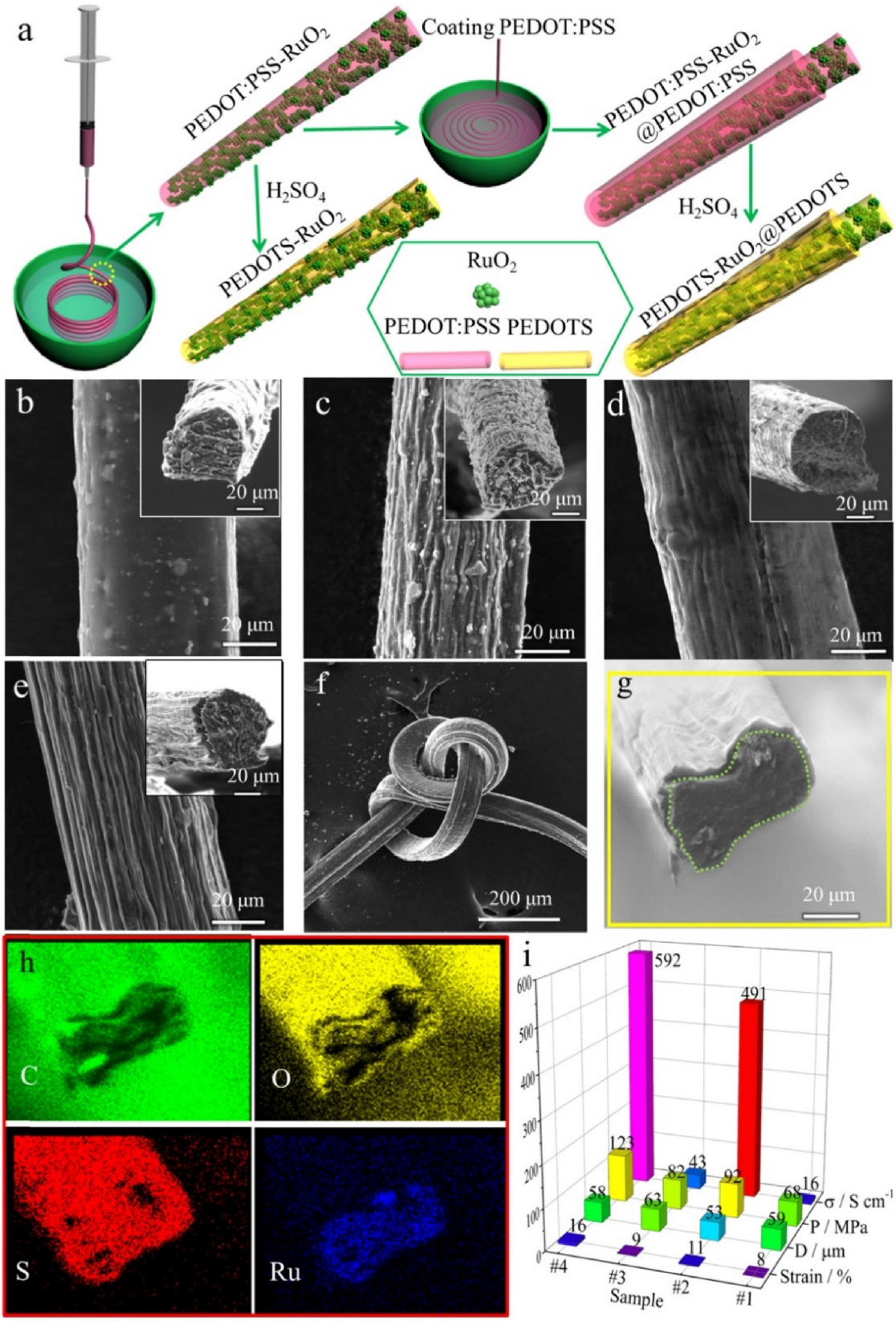

Fig. 8. (a) Schematic illustration of preparation processes of different fibers; SEM images of (b) PEDOT:PSS-RuO_2, (c) PEDOTS-RuO_2, (d) PEDOT:PSS-RuO_2@PEDOT:PSS and (e) PEDOTS-RuO_2@PEDOTS fiber, the insets are cross section images of corresponding fibers; (f) SEM images of a tied PEDOTS-RuO_2@PEDOTS fiber; (g, h) SEM and elemental mapping images of cross section of the PEDOTS-RuO_2@PEDOTS fiber; (i) 3D histogram of diameter, tensile strength, tensile strain and electrical conductivity of PEDOT:PSS-RuO_2 (#1), PEDOTS-RuO_2 (#2), PEDOT:PSS-RuO_2@PEDOT:PSS (#3) and PEDOTS-RuO_2@PEDOTS (# 4) fiber. Reproduced with permission [133]. Copyright 2018, Elsevier.

temperature range and further improved its electrical conductivity. Through their synergistic effects, the graphene-silver-PPy nanocomposite electrode demonstrated excellent conductivity, flexibility, and high capacity over a wide temperature range. When assembled into solid-state supercapacitors, it exhibited remarkable capacity and cycle stability from −45 °C to 80 °C.

Transition metal oxides and conductive polymers can synergize to form composites tailored for LTPCs. For example, Wang et al. [133] engineered a novel composite fiber material named PEDOT:PSS--RuO_2@PEDOTS for fiber supercapacitors, leveraging the conductive polymer PEDOT:PSS and the transition metal oxide RuO_2. The preparation processes of different fibers are presented in Fig. 8a. The as prepared PEDOT:PSS-RuO_2@PEDOTS fiber electrode featured a core-shell structure (Fig. 8e and **g**): the inner PEDOT:PSS-RuO_2 fiber (Fig. 8c) was fabricated through wet spinning of a mixture of PEDOT:PSS and RuO_2 solution, while the outer shell comprised a protective layer of PEDOT:PSS applied through additional dipping and coating in the PEDOT:PSS solution (Fig. 8d). Subsequent removal of most of the PSS from the surface, facilitated by sulfuric acid treatment, induced the rearrangement of PEDOT segments, enhancing intermolecular forces and resulting in the fiber electrode (PEDOT:PSS-RuO_2@PEDOTS) with increased tensile strength and conductivity (Fig. 8f and **i**). The well-dispersed amorphous RuO_2 nanoparticles (Fig. 8b and h) within the core contributed to higher pseudocapacitance, while the conductive polymer not only provided pseudocapacitance but also served as a current collector due to its high conductivity. Additionally, the conductive polymer coating on the shell acted as protection layer for RuO_2 nanoparticles, inhibiting structural disintegration and potential side reactions during cycling. Consequently, compared to an uncoated PEDOT:PSS-RuO_2 electrode, the PEDOT:PSS--RuO_2@PEDOTS electrode exhibited superior cyclic stability. In contrast, degradation occurred in the case of the PEDSS-RuO_2 electrode due to the pulverization and exfoliation of RuO_2 particles on the surface during cycling. The resulting fiber supercapacitor, composed of this electrode material and an aqueous gel electrolyte, exhibited a high energy density of 14.2 μWh cm^{-2} even at a low temperature of −60 °C. This strategy effectively harnesses the advantages of both conductive polymers and transition metal oxides, allowing the synthesized material to manifest high capacity and excellent temperature stability simultaneously. Table 3 summarizes the properties and performances of various LTPCs utilizing different electrode materials and optimization strategies, highlighting the effectiveness of these approaches.

3.2. Interface modification

The electrode-electrolyte interface, serving as the site for crucial interfacial processes encompassing ion transport and charge transfer, plays a pivotal role in dictating the electrochemical performance of supercapacitors. Consequently, it has consistently been a focal point of intensive research. For instance, Toupin et al. [134] employed various synthesis methods to obtain materials with diverse pore sizes and distributions for the fabrication of supercapacitors, followed by subsequent performance comparisons. The outcomes revealed that the specific capacitance of carbon materials decreased at low temperatures, and the presence of a substantial number of mesopores and macropores could enhance rate capability. However, they observed no straightforward correlation between pore size distribution and the capacitance of carbons. Further exploration is required to investigate the mechanism by which pores influence temperature-related capacitance. Subsequently, Xu et al. [26] identified that the decline in supercapacitor capacitance at low temperatures primarily stemmed from the sluggish ion diffusion at the solid-liquid interface, attributable to the deceleration of the ion desolvation process under lower temperatures. When solvated ions migrate from the electrolyte to the electrode, the ion desolvation process encounters hindrance in small pores. The solvation energy imposes a

Table 3
A summary of properties and performances of LTPCs.

Electrode	Electrolyte	Minimum Working Temperature (°C)	Capacity (Temperature, Compared to RT)	Cycling stability	Reference
PPy-N || PPy-N	PVA/H_2SO_4/H_2O/EG	−56	>50 F g^{-1} at 1 A g^{-1} (−50 °C, >40 %)	88.9 % after 1000 cycles (−50 °C)	[64]
1D $Ni(OH)_2$ nanorods || AC	NaCl/KOH/H_2O/EG	−30	203 F g^{-1} at 10 A g^{-1} (−30 °C, 61.1 %)	90.21 % after 10 000 cycles at 5 A g^{-1} (−30 °C)	[76]
InP_3//InP_3	PVA/H_3PO_4/H_2O	−25	27.2 F cm^{-3} at 5 mV s^{-1} (−25 °C, 69 %)	88.7 % after 10 000 cycles at 1 V s^{-1} (25 °C)	[80]
$Ti_3C_2T_x$	H_2SO_4 (40 wt%)	−60	79 mA h g^{-1} at 100 mV s^{-1} (−50 °C, >75 %)	7 % loss after 20 000 cycles at 40 A g^{-1} (−60 °C)	[9]
N-3DG/CNTs@Ni-MnO_2 || N-3DG/CNTs	PVA/$LiClO_4$	−20	46.4 F cm^{-3} at 30 mV s^{-1} (−20 °C, 70 %)	85.2 % retention after 10 000 cycles (−20 °C)	[90]
WO_3/CNT/KB || PBA/CNT/KB	H_2SO_4/H_2O/EG	−60	2.077 F cm^{-2} at 0.5 mA cm^{-2} (−60 °C, 61.3 %)	99 % after 10 000 cycles (−60 °C)	[92]
N-CFX	PVA/KOH/EG/H_2O	−20	38.6 F g^{-1} at 0.5 A g^{-1} (−20 °C, 87 %)	almost 100 % after 2000 cycles (−20 °C)	[103]
N/S-HPC ||N/S-HPC	PVA/KOH/H_2O	−20	~150 F g^{-1} at 10 A g^{-1} (−20 °C, small change)	small change after 1000 bends (−20 °C)	[106]
AC || MoO_{3-x} nanobelt	H_2SO_4/EG/H_2O	−25	138.4 F g^{-1} at 50 A g^{-1} (−25 °C, 46 %)	137 % after 50 000 cycles (−25 °C)	[118]
C/N-CNMA || AC	PVA/KOH/IPA	−30	9.48 Wh kg^{-1} at 875.08 W kg^{-1} (−20 °C)	90.35 % after 20 000 cycles (−20 °C)	[119]
Mn_3O_4—NPCN/CF || Mn_3O_4—NPCN/CF	PVA/KOH/H_2O	−20	142 F g^{-1} at 100 mV s^{-1} (−20 °C, 81.6 %)	nearly unchanged after 500 cycles (−20 °C)	[84]
GN/VGNS/MnO_2 || GN/VGNS/MnO_2	KOH/H_2O	−30	239 F g^{-1} at 1 A g^{-1} (−30 °C, 80.8 %)	86.0 % after 5000 cycles from −30 to 60 °C	[128]
CNT/PPy || CNT/PPy	PVA/H_3PO_4/H_2O	−27	32 F g^{-1} at 100 mV s^{-1} (−27 °C)	92 % after 5000 cycles at 200 mV s^{-1} (−27 °C)	[131]
PPy/AgGN || PPy/AgGN	PVA/H_2O/H_3PO_4	−45	611.5 F g^{-1} at 0.5 A g^{-1} (−45 °C, 76.15 %)	93 % after 3000 cycles at 200 mV s^{-1} (−45 °C)	[132]
PEDOT:PSS-RuO_2@PEDOTS || PEDOT:PSS-RuO_2@PEDOTS	PVA/LiCl/H_2O	−60	78.8 mF cm^{-2} at 50 mV s^{-1} (−60 °C, 43.9 %)	97.2 % after 5000 cycles at 50 mV s^{-1} (−60 °C)	[133]

PPy : Polypyrrole; PBA: Prussian blue analog; KB: Ketjenblack; *N*-CFX: N-doped carbon framework; N/S-HPC: nitrogen/sulfur-codoped hierarchically porous carbon materials; AC: active carbon; C/N-CNMA: C, N and Ag-doped layered Ni-Co-Mn ternary hydroxide IPA: isobutyl alcohol; Mn_3O_4—NPCN/CF: Mn_3O_4-embedded 3D N/P co-doped carbon cloth/carbon foam; GN/VGNS/MnO_2: Graphene Network/vertical graphene nanosheets/MnO_2.

barrier to ion desolvation, with the energy barrier increasing as the temperature decreases, thereby impeding ion diffusion at the interface. Therefore, optimizing pores to larger sizes can enhance performance by facilitating the entry of solvated ions into the pores. This conclusion was further substantiated by another pertinent study. Xu et al. [135] demonstrated that the desolvation of Li^+ during its insertion into a graphene electrode at the electrolyte/graphene interface constituted the primary energy-consuming step, i.e., the rate-determining step. Consequently, reducing the solvation energy is anticipated to augment ion interfacial diffusion.

The solvation energy of ions is contingent upon the charge carrier and its coordination environment, and it can be modulated through meticulous electrolyte design [136,137]. Investigating the impact of electrolyte salt ions, Nithya et al. [138] scrutinized the electrochemical performance of Bi_2WO_6 nanoparticles in various aqueous electrolytes (1 M LiOH, 1 M NaOH, 1 M KOH, 1 M $NaSO_4$, and 6 M KOH). The results revealed that K^+, with the smallest hydrated cation radius (3.31 Å), exhibited superior ion conductivity and current response compared to Na^+ (3.58 Å) and Li^+ (3.82 Å). This superiority can be attributed to the smaller hydrated ion radius, facilitating diffusion within the electrolytes. Furthermore, despite sharing the same charge number with Na^+, Li^+ and K^+ possesses a relatively larger radius, resulting in lower charge density, thereby weakening its solvation interaction with water molecules, favoring the desolvation of ions upon entering the electrode. Similar outcomes can be obtained for anions. Chae et al. [139] found that replacing larger anions (SO_4^{2-}) with smaller ones (Cl^-) can enhance capacity at high scanning rates. Notably, although K^+ has a larger crystal radius, it exhibits a smaller hydrous radius than Li^+ and Na^+. In contrast, both the crystal and hydrous radii of SO_4^{2-} are larger than those of Cl^-, owing to the less significant hydration of larger anions compared to that of smaller cations. Hence, the judicious selection of appropriate salts emerges as an effective strategy to regulate solvent solvation energy. Additionally, the solvent can influence the coordination environment of ions, thereby impacting solvation energy [140,141]. Xu et al. [136] investigated the desolvation energy of Li^+ in four different solvents, including 1,3-dioxane (DIOX), ethyl methyl carbonate (EMC), ethylene carbonate (EC), and dimethyl carbonate (DMC), through density functional theory (DFT) calculations. The results revealed that the desolvation energy of Li^+ in DIOX was the lowest, effectively enhancing the migration of Li^+ at the solid-liquid interface at low temperatures. Consequently, in this study, DIOX was employed as a solvent, enabling the assembled lithium-ion battery to operate at an ultralow temperature of −80 °C.

In addition to the influence of solvation, maintaining excellent wettability between electrolytes and electrodes is another essential factor that promotes the infiltration and penetration of the electrolyte into the electrode, enhancing the effective contact surface area. Two effective strategies for improving interfacial wettability involve modifying electrode materials and optimizing electrolytes. In terms of electrode modification, heterogeneous atom doping and structure design have proven effective in enhancing surface wettability. For instance, Shi et al. [142] employed a hydrothermal method and gas-phase phosphating treatment to achieve the in-situ growth of active material NiCoP/$NiCo_2N$ (NCPN) on carbon cloth, serving as the binder-free cathode. B, S co-doped bio--derived porous carbon was utilized as the anode. NCPN exhibited higher conductivity due to the absence of the binder, enabling direct electron transmission between the active substance and the current collector. Moreover, the binder-free feature of NCPN nanowires directly grown on carbon cloth enhanced hydrophilicity, facilitating ion diffusion. The contact angle between the electrolyte and the electrode was almost 180° for this configuration, compared to only 74° when coating the active substance slurry directly onto carbon cloth. Additionally, for the anode consisting of B, S co-doped biomass carbon material, doping with B and S introduced additional holes and free electrons into biomass carbon, promoting electron transport and providing more active sites. B, S co-doping also improved the wettability between the carbon electrodes and electrolytes. Considering the wettability of transition metal oxides, Wu et al. [118] introduced oxygen vacancies into MoO_3 to fabricate oxygen-rich MoO_{3-x} nanobelts and investigated their wettability with H_2SO_4/EG electrolyte compared to MoO_3 nanobelts. The results showed that the penetration rate of H_2SO_4/EG electrolyte in MoO_{3-x} nanobelts was ten times faster than that in MoO_3 nanobelts due to their increased interlayer spacing, good dispersity, and narrow structure. Furthermore, the enhanced wettability of MoO_{3-x} nanobelts allows for more efficient utilization of active sites, facilitating rapid proton (H^+) transport and enabling higher charge/discharge current densities. Moreover, wetting properties can be optimized by incorporating additives into the electrolytes. Liu et al. [143] successfully reduced the contact angle of the electrolyte on nonporous gold plate electrodes, achieving an enhancement in specific capacitance by introducing acetonitrile and isopropyl acetate to ionic liquids. The universality of this approach was examined using carbon-based electrodes, revealing that augmenting the wetting properties of the electrolyte on the electrode through propyl alcohol addition to potassium hydroxide electrolyte resulted in increased capacitance and prolonged cycle life for assembled supercapacitors, underscoring the significance of electrode-electrolyte compatibility in designing high-performance supercapacitors.

3.3. Electrolyte modulation

The electrolytes employed in supercapacitors can be broadly classified into three categories: aqueous electrolyte, organic electrolyte, and ionic liquid electrolyte. In low-temperature environments, each type presents distinct advantages and limitations. Aqueous electrolytes offer high conductivity, low viscosity, and non-flammability; however, their higher melting points and propensity to freeze at low temperatures constrain their utility in cold environments. In contrast, organic electrolytes possess lower melting points and broader voltage windows, yet their larger molecular sizes necessitate electrodes with larger pores [144]. Furthermore, organic electrolytes exhibit increased viscosity and reduced conductivity in low-temperature conditions. Additionally, many organic electrolytes are characterized by toxicity, volatility, and flammability, contributing to inadequate safety performance. Ionic liquids or room temperature molten salts maintain fluidity over a wide temperature range, presenting potential applications in low-temperature supercapacitors. In comparison to organic electrolytes, they offer wider voltage windows (up to 3.5 V), non-volatility, and non-flammability [145]. However, ionic liquids often exhibit high viscosity and very low self-diffusion coefficients of ions, resulting in significantly diminished ion conductivity despite high charge carrier concentrations. Therefore, it becomes imperative to employ suitable strategies for electrolyte modulation in low-temperature environments. These strategies may include the utilization of water in salt, the incorporation of additives or co-solvents, and the introduction of gels into electrolytes (Table 4) [146].

3.3.1. Water in salt

The implementation of high concentrations of salt in water, known as the Water-in-Salt (WIS) strategy, provides a straightforward approach to concurrently lower the freezing point of the electrolyte and enhance its conductivity. This strategy has found extensive application in low-temperature aqueous supercapacitors [9,15]. For instance, Zhu et al. [13] employed a concentrated LiCl hydrogel electrolyte with a high concentration of 20 mol kg^{-1} in MXene-based supercapacitors. In comparison to a 1 mol LiCl electrolyte with a freezing point of −26 °C, the 20 mol concentrated LiCl electrolyte exhibited a significantly lower freezing point of −57 °C, demonstrating exceptional performance at low temperatures and enabling efficient operation of the assembled supercapacitor at −40 °C. The observed decrease in freezing point in highly concentrated LiCl solutions was explained by Raman spectroscopy results. In a 1 mol LiCl solution, Li^+ ions are solvated by four water molecules and well separated by Cl^- ions. At low temperatures, a large number of free water molecules tend to form hydrogen bond networks, making them susceptible to freezing. However, as the concentration of

Table 4
The composition, freezing point, ionic conductivity and operation temperature of electrolytes for LTPCs.

Composition	Freezing point (°C)	Ionic Conductivity	Operation Temperature (°C)	Reference
20 mol kg^{-1} LiCl in H_2O	−57	69.5 mS cm^{-1}	−40	[13]
20 mol kg^{-1} LiTFSI in H_2O			−20	[147]
5 mol kg^{-1} LiTFSI in H_2O		17.4 mS cm^{-1}	−30	[50]
$NaClO_4$ in H_2O/AN (1.7:4.7:3, molar ratio)		4.95 mS cm^{-1}	−50	[51]
$(NH_4)_2SO_4$ in H_2O/EG (1:1, mass ratio)			−30	[150]
2 M $LiNO_3$ in H_2O/DMSO (10:90, mass ratio)	−130.1	0.16 mS cm^{-1} at −40 °C	−40	[154]
6.6 mol kg^{-1} LiTFSI in H_2O/DMSO (2:1, molar ratio)	−140	2.97 mS cm^{-1}	−35	[157]
1.2 M TEMA TFB in 30 vol% EA + 70 % AN	−65.4	~7 mS cm^{-1} at −60 °C	−60	[159]
$LiClO_4$ in 42 vol% DMF + H_2O (molar ratio of $LiClO_4$ to H_2O is 1:0.5)		9.3 mS cm^{-1}	−20	[160]
1 M $EMIMBF_4$/TEP		5.2 mS cm^{-1} at −20 °C	−20	[161]
ChCl/EG (1:2, molar ratio)		11.75 mS cm^{-1}	−40	[167]
ChCl/EG/urea (1:2:1, molar ratio)	−113	6.33 mS cm^{-1} at −40 °C	−40	[168]
4 M LiCl in PVA/H_2O	<-50	40.1 mS cm^{-1} at −40 °C	−40	[83]
LiCl in PVA/H_2O/EG (H_2O/EG 2:1, mass ratio)	<-40	2.38 mS cm at −40 °C	−40	[189]
2M LiCl in P($AMPS_{0.3}$-co-$AAM_{0.4}$)/H_2O/DMSO (24:, volume ratio)	−39.5	0.82 S m^{-1} at −20 °C	−20	[190]
KCl in SF/EMImAc/H_2O	−68	0.016 S m^{-1} at −50 °C	−50	[191]

TEMA TFB: Methyl triethylammonium tetrafluoroborate; EA: ethyl acetate; AN: acetonitrile; DMF: *N,N*-dimethylformamide; TEP: triethyl phosphate; $EMIMBF_4$: 1-butyl-3-methylimidazolium tetrafluoroborate; ChCl: choline chloride; AMPS: 2-acrylamido-2-methypropane sulfonic acid; AAM: acrylamide; P($AMPS_{0.3}$-co-$AAM_{0.4}$): 0.3 and 0.4 represents the mass ratios of AMPS/AAM; DMSO: dimethyl sulfoxide; SF: silk fibroin; EMImAc: 1-ethyl-3-methylimidazolium acetate.

LiCl gradually increases, more water molecules coordinate with Li^+, leading to a reduction in free water clusters. At a 20 mol concentration, most water molecules are coordinated with Li^+ through oxygen ions, resulting in minimal hydrogen bonds. Due to the solvation effect of abundant Li^+ ions, the high-concentration gel electrolyte of 20 mol exhibits a low freezing point of −57 °C. Furthermore, employing this high-concentration salt strategy allowed for an extended electrochemical stability window up to 2.7 V (−1.5 to 1.2 vs. Ag/AgCl), while being only 1.9 V for the 1 mol LiCl solution. Through both in-situ and ex-situ characterizations, the authors discovered distinct energy storage mechanisms for MXene electrodes when using the 20 M LiCl WIS (Water--in-Salt) electrolyte compared to the 1 M LiCl electrolyte. The high concentration of LiCl electrolyte promoted anion intercalation to regulate interfacial reaction kinetics and inhibited the oxidation of MXene, thereby expanding the voltage window for MXene in aqueous electrolytes. Moreover, the insertion/extraction of ions between MXene layers in high-concentration electrolytes enabled MXene with excellent cycling performance.

However, several studies have indicated that the application of the WIS strategy at low temperatures introduces certain challenges, such as salt precipitation and increased viscosity in high-concentration salt solutions. For instance, Xu et al. [147] explored the temperature dependence of carbon-based supercapacitors utilizing WIS electrolytes. They assembled supercapacitors with varying concentrations of LiTFSI electrolyte and carbon electrodes to investigate the impact of WIS electrolyte concentration and temperature on supercapacitor performance. The findings revealed that at a high temperature of 60 °C, a 20 M LiTFSI electrolyte exhibited optimal performance. Conversely, at a low temperature of −10 °C, a relatively lower concentration of 5 M LiTFSI electrolyte demonstrated superior performance. At room temperature, a lower concentration of 5 M LiTFSI showed lower impedance compared to a 20 M LiTFSI solution. This discrepancy in performance is attributed to increased ion interaction at excessive concentrations, hindering the transport of electrolyte ions to the electrode and membrane pores, as well as impeding charge transfer at the electrode/electrolyte interface. Therefore, when employing the WIS strategy, it is imperative to select an appropriate concentration based on the operational temperature range. For lower temperatures, a lower electrolyte concentration is advisable, while for higher temperatures, a higher electrolyte concentration is preferable.

To mitigate the challenges associated with salt precipitation, high viscosity, and low conductivity arising from a concentrated salt solution, Dou et al. [50] introduced acetonitrile as a co-solvent into the LiTFSI WIS electrolyte. This resulted in the formation of an "acetonitrile/water in salt" (AWIS) mixed electrolyte, effectively reducing viscosity and enhancing conductivity. The incorporation of acetonitrile regulated the tight coordination between anions and cations in the LiTFSI WIS electrolyte, diminishing their attraction and improving ion dynamics. Furthermore, AWIS exhibited superior diffusion capabilities for both anions and cations compared to the 21 M LiTFSI WIS, particularly at lower concentrations of 5 M LiTFSI. It demonstrated twice the ion conductivity while maintaining lower viscosity (below 10 %), leading to supercapacitors with reduced impedance even at −30 °C. This approach not only enhances electrochemical performance but also reduces the required amount of LiTFSI salt, achieving cost reduction without compromising performance. Additionally, the electrolyte remains liquid even at −50 °C, enabling assembled devices to exhibit a high rate capability of 8.6 F g^{-1} at 10 A g^{-1} under −30 °C conditions. Furthermore, Sun et al. [51] investigated the mechanism of acetonitrile inhibition on salt precipitation by introducing acetonitrile into a $NaClO_4$-based WIS electrolyte. Theoretical calculations and experimental analysis revealed that acetonitrile molecules strongly coordinate with Na^+ ions, resulting in alterations in the solvation structure of both cations and anions while weakening the interaction forces between them. This effectively inhibits the formation of $NaClO_4$ cation-anion pairs, demonstrating the efficacy of disrupting the attraction between anions and cations in inhibiting salt precipitation.

3.3.2. *Additives/Co-solvent*

Owing to the inherent constraints of a singular solvent in meeting the dual criteria of low melting point and high electrical conductivity at lower temperatures, a prevalent approach involves augmenting electrolyte properties—such as freezing point, ionic conductivity, viscosity, dielectric constant, voltage window, among others—by introducing additives or co-solvents.

To enhance the freeze resistance of aqueous electrolytes with elevated melting points, the incorporation of lower-melting organic compounds as antifreeze additives or co-solvents is a common practice. Examples of such compounds include methanol [148,149], acetonitrile [50], ethylene glycol [150], and acetone [151]. In a study by Alexander et al. [150], the freezing point of water-based solutions was effectively reduced by

incorporating ethylene glycol, thereby enabling the application of supercapacitors in low-temperature environments. The investigation explored the influence of different mass concentrations of ethylene glycol (ranging from 0 % to 50 %) on the properties and electrochemical performance of Na_2SO_4, Li_2SO_4, K_2SO_4, and $(NH_4)_2SO_4$ aqueous electrolytes. To prevent precipitation at low temperatures, the electrolyte concentration was maintained at 80 % of its saturation concentration at 0 °C. The introduction of ethylene glycol significantly lowered the freezing point; for instance, a Li_2SO_4 aqueous solution that froze at −10 °C remained liquid at −30 °C when supplemented with 30 % ethanol. However, it was observed that increasing ethylene glycol content resulted in reduced solubility of all four salts. Moreover, as the content of ethylene glycol increased and temperature decreased, the viscosity of the electrolyte visibly increased. Consequently, a higher ethylene glycol content impeded ion mobility within the electrolyte solution, particularly in pore structures, leading to slower kinetics and restricted mass transfer processes, as evidenced by distinct deviations in cyclic voltammetry curves under high scan rates.

Moreover, specific organic compounds with higher freezing points can function as additives in aqueous electrolytes to manipulate the hydrogen bond network within the electrolyte, thereby achieving a reduced freezing point. Dimethyl sulfoxide (DMSO) [152,153] and cholinium chloride (ChCl) are examples of compounds employed for this purpose. Wu et al. [154] tailored the low-temperature performance of a 2 M $LiNO_3$ aqueous electrolyte solution by introducing DMSO as an antifreeze additive. Owing to its strong polarity, DMSO can establish robust solvation interactions with Li^+ ions and form substantial hydrogen bonds with water molecules, disrupting the original hydrogen bonds between water molecules and preventing their freezing [155,156]. Molecular dynamics simulations further verified that increasing concentrations of DMSO in the electrolyte resulted in a reduction in hydrogen bonds between water molecules, with a concomitant dominance of $1H_2O$-2DMSO molecular aggregates. Under these influences, the incorporation of DMSO antifreeze additive lowered the freezing point of the $LiNO_3$-H_2O-DMSO electrolyte to below −120 °C, while maintaining a favorable ion conductivity of 0.16 mS cm^{-1} at −40 °C, thereby promoting enhanced electrochemical performance. Similarly, Lu et al. [157] utilized a cosolvent comprising DMSO and water, along with an electrolyte containing LiTFSI salt, to develop low-temperature supercapacitors. The DMSO-H_2O cosolvent in a molar ratio of 2:1 exhibited an impressively low freezing point of −140 °C. This substantially reduced melting point renders this mixture highly suitable for operation in extremely cold environments.

Similarly, the cosolvent strategy is employed to optimize organic electrolytes, as a single organic solvent often struggles to simultaneously meet the criteria of low melting point, high ionic conductivity, non-flammability, and electrochemical stability. For example, acetonitrile exhibits favorable electrochemical stability and ion conductivity at low temperatures, but its toxicity and flammability present significant safety risks. On the other hand, propylene carbonate is considered safe but demonstrates higher viscosity at lower temperatures, adversely affecting its ion conductivity [158]. Consequently, solvent mixtures are commonly utilized to enhance the properties of organic electrolytes. For instance, Galimzyanov et al. [159] investigated the impact of introducing cosolvents on the properties of an electrolyte comprising methyl triethyl tetrafluoroborate ammonium (CH_3) $(C_2H_5)_3NBF_4$ (TEMA·TFB) salt and acetonitrile as solvents. The cosolvents used included ethyl acetate (EA), propyl acetate (PA), and butyl acetate (BA). The results revealed that the electrolyte system composed of 1.2 M TEMA·TFB salt mixed with a 30 % volume fraction of EA in acetonitrile exhibited an extended operating temperature range and enhanced electrochemical stability, demonstrating optimal electrochemical performance. This can be attributed to the exceptional electrochemical stability and moderate polarity of EA, as well as its low melting point and viscosity. Compared to PA and BA, EA possesses superior characteristics due to its moderate molecular weight. Too low a molecular weight would result in an increased boiling point, while too high a molecular weight would increase viscosity and decrease conductivity. Fortunately, EA has an appropriate viscosity to maintain a higher boiling point and exhibits good conductivity at low temperatures. The supercapacitor composed of the hybrid electrolyte exhibited excellent performance over a wide temperature range from −60 to +60 °C, maintaining more than 90 % of room-temperature capacitance even at an extremely low temperature of −60 °C. Considering the flammability of organic solvents, some researchers adopt flame-retardant solvents such as water to form a cosolvent with organic solvents [160]. Li et al. [161] reported a triethyl phosphate (TEP)-based binary electrolyte with non-flammability. TEP is one type of organic phosphates, widely used as flame-retardant additives in alkali metal ion batteries due to their flame retardancy, wide electrochemical window, and low viscosity. The introduction of TEP effectively imparts the electrolyte with a non-flammable property, enhancing the safety of the device. Moreover, the interionic hydrogen bonds of 1-butyl-3-methylimidazolium tetrafluoroborate ($EMIMBF_4$) were effectively broken/weakened by TEP as the P=O bonds of TEP can interact with H sites of imidazolium. Therefore, the introduction of TEP also reduces the viscosity of ionic liquids and improves the mobility of ions, enabling supercapacitors composed of the electrolyte to be used at low temperatures of −20 °C. This study also demonstrates the effectiveness of cosolvents composed of organic solvents and ionic liquids in optimizing electrolytes.

The cosolvent strategy is also employed to optimize the properties of electrolytes based on ionic liquids [162]. Yambou et al. [163] investigated the physical and chemical properties of three binary ionic liquids formed by mixing 1-ethyl-3-methylimidazolium $[EMIm]^+$ cations with fluoride anions, including bis(fluorosulfonyl)imide $[FSI]^-$, bis(trifluoromethanesulfonyl)imide $[TFSI]^-$, and tetrafluoroborate $[BF_4]^-$. The mixed ionic liquids were $[EMIm][TFSI]_xFSI$, $[EMIm][FSI]_xBF_4$, and $[EMIm][TFSI]_xBF_4$. Various properties including density, viscosity, conductivity, and ionicity were investigated by the researchers. The results demonstrated a significant reduction in freezing point when different ionic liquids were mixed. This approach effectively yielded 17 low-temperature mixtures, which remain liquid down to ∼ −90 °C, contrasting with the relatively high crystallization and melting temperatures of the parent ionic liquids. Additionally, the mixtures of different pure components exhibited different trends in viscosity changes. Compared to parent components, $[EMIm][TFSI]_xFSI$ and $[EMIm][TFSI]_xBF_4$ presented higher viscosity, contrary to the case of $[EMIm][FSI]_xBF_4$. The different trend of viscosity changes can be attributed to significant differences in their ionic structures and steric effects contributing to ion organization. Interestingly, the conductivity and viscosity of ionic liquids exhibit an abnormal correlation. For example, despite having higher viscosity than [EMIm][TFSI], $[EMIm][BF_4]$ demonstrated higher conductivity, attributed to other factors influencing conductivity, such as ionic size, charge delocalization, and density [164]. The conductivity of mixed compositions fell between those of the two pure components and increased with a higher proportion of the more conductive component. Among them, $[EMIm][FSI]_{0.5}$ $[BF_4]_{0.5}$ and $[EMIm][FSI]_{0.6}$ $[BF_4]_{0.4}$ displayed the lowest viscosity and highest conductivity, making them suitable for manufacturing supercooling supercapacitors operating at −40 °C. It is worth noting that deep eutectic solvent (DES), as a special ionic liquid, exhibits unique properties. It is formed by mixing different solvents that can serve as hydrogen bonding donors and acceptors, resulting in hybrid solvents exhibiting lower melting points than the pure components, rendering it highly suitable for applications in LTPCs [165,166]. For instance, Zhong et al. [167] synthesized a DES by mixing choline chloride and ethylene glycol to be utilized in supercapacitors with a wide operational temperature range. Choline chloride acted as the hydrogen bond acceptor, while ethylene glycol functioned as the hydrogen bond donor. The authors investigated the characteristics of the mixed solution at three different molar ratios of 1:1, 1:2, and 1:3 for ChCl to EG. The results demonstrated that this DES exhibited excellent conductivity along with low viscosity when the molar ratio is 1:2. Additionally, DFT calculations were conducted on the

adsorption energies of these three ratios. Higher absolute values of adsorption energies indicate enhanced system stability and correlation with transport properties such as viscosity and ion conductivity. The results revealed that the absolute values of adsorption energies for ChCl to EG at molar ratios of 1:1, 1:2, and 1:3 were 3.69 eV, 4.42 eV, and 4.30 eV, respectively, confirming the superior stability of the molar ratio of 1:2. Furthermore, in another study, the authors introduced urea into the binary DES composed of choline chloride and ethylene glycol [168]. Analysis using Raman spectroscopy and infrared spectroscopy revealed strong evidence for intermolecular hydrogen bonding among these three constituents within the electrolyte system, predominantly involving chlorine atoms from ChCl interacting with hydrogen atoms derived from both EG hydroxyl groups and urea amino groups. Researchers investigated the differences in properties of electrolytes under different ratios. The results showed that at a molar ratio of 1:2:1 (ChCl: EG: urea), the electrolyte exhibited optimal transport characteristics at −40 °C, with low viscosity (<13 cP) and high conductivity (6.33 mS cm^{-1}). DFT theoretical calculations further confirmed that the electrolyte achieved maximum adsorption energy (24.66 eV) and optimal ion diffusion coefficient at this ratio. Compared to binary mixtures of ChCl and EG, this electrolyte demonstrated superior performance in a low-temperature environment of −40 °C, including higher energy density of 36.63 Wh kg^{-1} and a larger specific capacitance of 160 F g^{-1} at 1 A g^{-1}.

High-entropy materials are gaining increased attention in the field of electrochemistry due to their distinctive characteristics. For example, high entropy oxides have been widely used in the research of supercapacitors, batteries, and solid oxide fuel cells [169]. In addition, high entropy strategies can also be applied to the development of electrolytes. High-entropy electrolyte (HEE) has emerged as a novel hybrid electrolyte in recent years, gaining significant attention in the field of electrochemical energy storage research [170]. Comprising a single salt and various solvents or multiple salts dissolved in one solvent, HEE exhibits enhanced disorder within its internal ion or molecule composition, resulting in higher entropy and manifesting numerous distinctive properties such as reduced freezing point, increased solubility, improved kinetic performance, and enhanced stability [171–173]. Thermodynamically, the temperature of the liquid phase is determined by the Gibbs free energy of solid and liquid phases. Lowering the Gibbs free energy can effectively decrease the freezing point temperature. Based on the thermodynamic equation:

$$G = H - TS \tag{6}$$

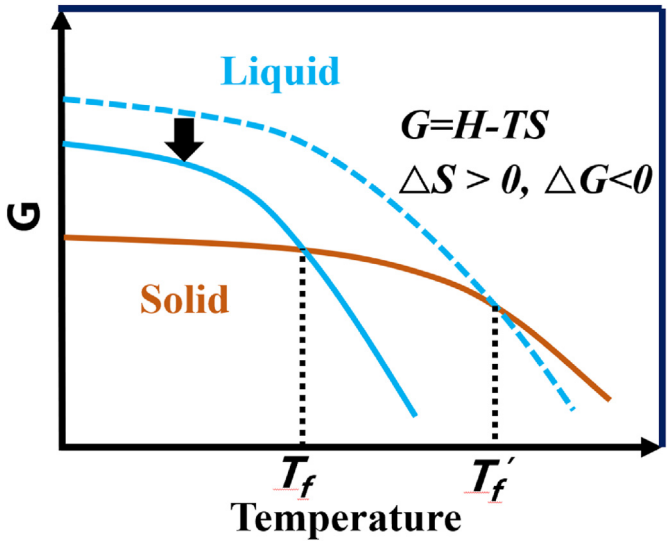

Fig. 9. Relationship between Gibbs free energy, entropy of liquid and the freezing point, in which S represents entropy of systems.

The Gibbs free energy (G) is defined by the enthalpy (H), thermodynamic temperature (T), and entropy (S) of a system. By increasing the entropy of the system through the utilization of more than one salt or solution, it becomes possible to reduce the Gibbs free energy and subsequently lower the freezing point (Fig. 9). This principle has led to the development of HEE systems, which have garnered attention in electrochemical energy storage research due to their unique advantages. In the context of low-temperature applications for various metal-ion batteries, HEE has demonstrated notable benefits. For instance, Yang et al. [174] synthesized $Li_2ZnCl_4{\cdot}9H_2O$ HEE by introducing LiCl as a supporting salt into a $ZnCl_2$ aqueous solution in an appropriate ratio. This electrolyte exhibited a low melting point and high ionic conductivity, enabling a zinc-ion battery to maintain 80 % of its room-temperature power density even at an extremely low temperature of −60 °C. The introduction of LiCl played a crucial role in facilitating the coordination of $ZnCl_2$ with additional Cl^- ions, leading to the formation of a preferred tetrahedral coordination structure of $ZnCl^{4-}$ anions. This reduced the prevalence of edge-shared Cl^- ions between Zn^{2+} and limited the formation of contiguous $[Zn_{4-m}^{2-m}]_n$ ($n > 3$) extended networks, thus enhancing ion conductivity. The optimal molar ratio of LiCl to $ZnCl_2$ (2:1) induced a significant change in solvation structure and entropy. At this ratio, extended $[Zn_{4-m}^{2-m}]_n$ ($n > 3$) aggregates underwent disruption into a wide distribution of shorter aggregates ($n \leq 3$), breaking the hydrogen bonding networks within the free solvent and excluding water from Zn^{2+} solvation. Simultaneously, Li^+ maintained strong coordination with water molecules, breaking down hydrogen bonds in water. Consequently, a unique frustrated solvation structure with high entropy was formed, contributing to high ionic conductivity at low temperatures and suppressing solvent crystallization. While HEE has demonstrated promising advantages in low-temperature applications for electrochemical energy storage devices, its application in low-temperature supercapacitors remains an area requiring further investigation and research expansion.

3.3.3. Gel framwork

Incorporating gel into electrolytes stands as a viable strategy for the development of LTPCs. Frequently employed gel materials encompass organic polymers such as poly (vinyl alcohol) (PVA) [175–177], acrylamide (PAM) [178,179], and pluronic [180]. The three-dimensional porous gel network established within the electrolyte serves to regulate molecular interactions and furnish transport channels, endowing it with characteristics akin to both liquids and solids. These include high conductivity, imperviousness to leakage, robust mechanical strength, an expanded voltage window, and resistance to low temperatures [181–183]. However, conventional hydrogel electrolytes, while manifesting advantageous properties, contain a notable proportion of water and are susceptible to freezing at lower temperatures. Consequently, gel electrolytes are typically utilized in conjunction with antifreezing strategies such as Water-in-Salt (WIS), additives, co-solvents, etc., to enhance their resistance against freezing [184,185]. Yet, it is imperative to carefully weigh the potential drawbacks associated with each strategy. For instance, elevated concentrations of salt are prone to causing the salting out phenomenon at lower temperatures, rendering the flexible hydrogel rigid and compromising ion migration. Moreover, this may impede the self-healing capability of the hydrogel, thereby affecting its overall durability and lifespan [186,187]. In the context of applying the co-solvent strategy to hydrogel electrolytes, although the introduction of organic solvent can influence the hydrogen bonds between water molecules and thereby reduce the freezing point, the presence of the organic solvent may hinder ion transport within the gel electrolyte, resulting in diminished ion conductivity [188].

For instance, Yin et al. [83] devised a Polyvinyl Alcohol/Lithium Chloride (PVA/LiCl) hydrogel electrolyte for a LTPC based on MXene by judiciously selecting an appropriate salt and concentration. The synthesis of PVA/LiCl involved a straightforward freeze-thaw process of a PVA and LiCl mixture, strategically preventing the formation of hydrogen bonds

between PVA chains, given that Li^+ ions can bind to the -OH groups of PVA chains. Consequently, the resulting PVA/LiCl hydrogels possess a low crosslinking density, imparting excellent flexibility. Furthermore, the introduction of a highly concentrated LiCl solution into the gel exhibited remarkable resistance to freezing and ion conduction capabilities. With LiCl concentrations reaching 1M and 2M, the freezing point diminished to −25.22 °C and −42.64 °C, respectively. Beyond 3M concentration, the solution remained unfrozen even at −50 °C. Moreover, heightened concentrations contributed to increased ionic conductivity, attributed to the augmented concentration of charge carriers and a loosely cross-linked structure resulting from the high LiCl concentration, facilitating pathways for ion transport. The ionic conductivity of PVA/LiCl hydrogels ascended from 1.2 to 128.3 mS cm^{-1} with the LiCl concentration increasing from 0 to 5M. Additionally, the issue of salt precipitation induced by high concentration salt solutions was effectively mitigated. Li^+ and Cl^- ions directly bound to the PVA chains, introducing additional charges to the PVA chain and preventing salting out. Furthermore, the loose cross-linked structure of the gel electrolyte generated a substantial number of active hydroxyl groups, fostering robust adhesion forces and enabling an effective and stable interface contact between the electrolyte and interface. Capitalizing on these synergistic characteristics, the MXene-based LTPCs fashioned with this electrolyte demonstrated a high specific volume of 113.13 mF cm^{-2} even at a frigid temperature of −40 °C.

In a separate investigation, Rong et al. [189] employed the cosolvent strategy to fabricate organic gel electrolytes incorporating PVA networks, a binary mixed solution of H_2O/EG, and LiCl salt. The binary mixed solution of H_2O/EG not only demonstrated a lower freezing point but also exhibited excellent solubility for LiCl, resulting in exceptional conductivity and anti-freezing properties of the gel electrolyte. Furthermore, solvent molecules could interact with PVA chains, thereby enhancing the mechanical performance and anti-freezing ability of the gel electrolyte. The researchers conducted a comparative analysis of the mechanical properties, anti-freezing performance, and conductivity between pure water gels and the organic gels. The findings indicated that even at −40 °C, the organic gel maintained good flexibility, whereas the water gel electrolyte solidified into a brittle state. At temperatures below −20 °C, the conductivity of the water gel approached zero, rendering it practically non-functional, while the organic gel electrolyte exhibited a high ionic conductivity of 2.38 mS cm^{-1}, showcasing promising applications in low-temperature environments. However, it was noted that despite the significant reduction in the freezing point with the introduction of EG, achieving higher ionic conductivity simultaneously remained challenging. In another exploration, Liu et al. [190] enhanced the anti-freezing performance of hydrogel electrolytes by incorporating DMSO as an antifreeze additive. Due to the formation of hydrogen bonds among polymer chains, DMSO, and water molecules, the polymer hydrogel exhibited stable mechanical properties and high ion conductivity over a broad temperature range, maintaining a high ion conductivity of 0.82 S m^{-1} at −20 °C. Owing to the low volatility, viscosity, strong polarity, and high dielectric constant of DMSO, its content influenced the electrochemical performance of the hydrogel electrolyte at low temperatures. When the volume ratio of H_2O/DMSO was 24:1, the resulting supercapacitor retained over 90 % of its room temperature capacity at −20 °C. However, insufficient DMSO content resulted in inadequate hydrogen bonding with polymer chains and water molecules, leading to lower capacity, while excessive DMSO could form dimers and reduce capacity at low temperatures.

Ionic liquids can be employed in the formulation of gel electrolytes, as demonstrated by Wang et al. [191], who synthesized a novel gel electrolyte SF/EMImAc/H_2O consisting of silk fibroin (SF), ionic liquid (EMImAc), water, and inorganic salt (KCl). This gel electrolyte exhibits outstanding water retention and anti-freezing capabilities. The strong interaction between EMImAc and water molecules in the SF/EMImAc/H_2O hydrogel electrolyte results in a significantly lower melting point of −68 °C compared to the traditional PVA/KCl hydrogel, which freezes at −16 °C. Furthermore, the SF/EMImAc/H_2O hydrogel electrolyte maintains an ionic conductivity of 0.016 S m^{-1} at a low temperature of −50 °C, whereas PVA/KCl cannot be detected at −30 °C. Additionally, owing to its robust hydrophilic and non-volatile properties, EMImAc enhances the water retention ability of the gel electrolyte. These distinctive features enable the supercapacitors assembled with this electrolyte to operate effectively at extremely low temperatures of −50 °C.

3.4. Thermal-assist LTPCs

In addition to enhancing the intrinsic low-temperature resilience of the device, thermal assistance represents another effective approach to ameliorate electrochemical performance in cold environments by directly adjusting the operational temperature of the device. External heating can substantially elevate the operational temperature of electrochemical energy storage devices, thereby augmenting their electrochemical performance under low-temperature conditions [192,193]. However, this method necessitates supplementary equipment to supply electrical energy for heating, thereby escalating the overall system cost. Self-heating, on the other hand, presents an alternative means to regulate operational temperatures without the reliance on external heating devices. This approach has demonstrated efficacy in the context of lithium-ion batteries. Wang et al. [194] eliminated the requirement for additional heating devices by devising a distinctive structure for lithium-ion batteries. They harnessed the ohmic heat generated by nickel foils in the activation circuit to raise the temperature of lithium-ion batteries during low-temperature conditions. Once elevated to an optimal temperature, a surface temperature-controlled switch facilitated the transition to a conventional working circuit with low internal resistance, characteristic of high-power output in lithium-ion batteries. This strategy effectively achieves self-heating, improving the working temperature without the need for supplementary heating equipment. However, the augmented complexity resulting from additional structural design and control systems, coupled with the energy consumption for self-heating, introduces potential challenges such as a reduction in energy density.

The photothermal-assisted heating strategy, heralded for its eco-friendly and sustainable attributes, obviates the need for additional equipment and energy consumption, garnering escalating interest. This method has demonstrated efficacy in the realm of low-temperature supercapacitors, involving the application of photothermal materials with notable conversion efficiency to convert solar energy into thermal energy, thereby heating electrochemical energy storage devices. For instance, Sun et al. [195] achieved self-heating of micro-supercapacitors (MSCs) by affixing a graphene photothermal film on the backside of the MSC. This straightforward strategy elevated the actual operating temperature of the MSC to −16.5 °C under 1 sun radiation in a low-temperature environment of −50 °C, thus significantly amplifying the electrochemical performance of MSC at low temperatures. In a similar study, Ma et al. [196] utilized a spinel-type transition metal oxide, $Cu_{1.5}Mn_{1.5}O_4$, as the coating material on supercapacitors. Due to the high photothermal conversion efficiency of the $Cu_{1.5}Mn_{1.5}O_4$ film, its effective operating temperature increased substantially by approximately 60 °C at −30 °C.

Given that coating the surface with photothermal materials can augment the weight of the device without a commensurate increase in its capacity, thereby diminishing the energy density of the device, some researchers have explored the utilization of materials with inherent photothermal conversion capabilities as electrode materials for supercapacitors. For example, Chen et al. [197] employed bifunctional TiN material in the construction of LTPCs. The TiN nanocrystals exhibit not only electrochemical activity but also exceptional photothermal conversion efficiency (62.5 %) and extensive light absorption (>98 %) across the entire solar spectrum. This characteristic facilitated an increase in the effective operating temperature to −10.8 °C in a low environment of

−36.6 °C under 1 solar illumination. Consequently, the assembled supercapacitors maintained 70.9 % specific capacitance and 59.3 % energy density at −40 °C compared to their room temperature performance. In a different study, Yu et al. [198] devised a photothermally active electrode for supercapacitors composed of 3D porous graphene and polypyrrole with a meticulously designed light absorption structure. The distinctive electrode structure, coupled with the planar configuration of the micro-supercapacitor, resulted in high sunlight absorption and effective low radiation electron relaxation dynamics. The electrode material exhibited high photothermal conversion efficiency due to its elevated light absorption rate (>98 %) and photothermal conversion efficiency (23.5 %). Under one solar irradiation at −30 °C, the assembled micro-supercapacitor experienced a 4.08-fold increase in specific capacitance, reaching 520 mF cm^{-2}, comparable to its room-temperature performance. Therefore, the strategy of photothermal-assisted heating proves effective in enhancing the electrochemical performance of supercapacitors at low temperatures. It is pertinent to note that the reliance on solar energy renders this strategy particularly suitable for regions with abundant and stable solar resources, while its applicability is constrained in areas with limited solar energy.

4. Conclusions and outlook

This comprehensive review explores the topic of LTPCs, focusing on strategies to maintain energy storage performance in supercapacitors under extreme cold conditions (Fig. 10). It explores novel electrode materials designed strategies to improve energy storage efficiency under such conditions. Additionally, the paper examines the optimization methods of electrolytes, including aqueous electrolytes, organic electrolytes and ionic liquids-based electrolytes. Commonly used strategies include water in salt, additives/cosolvents and introduction of gel, all geared towards improving the low-temperature performance of energy storage devices. Furthermore, innovative approaches such as self-heating mechanisms and solar-thermal conversion coatings are discussed to augment energy storage capacity in supercapacitors operating at low temperatures. In essence, this study offers valuable insights into the development of robust energy storage systems capable of operating effectively in challenging environmental conditions.

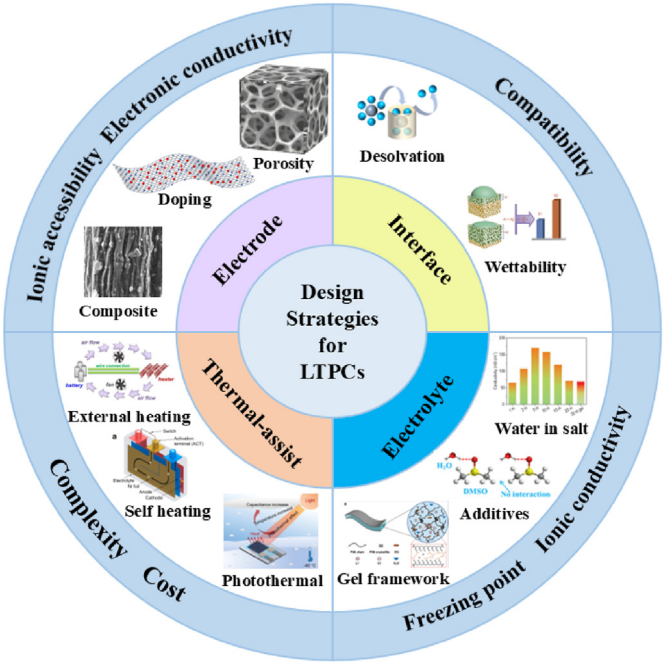

Fig. 10. A summary of the design strategies for LTPCs. (Composite, reproduced with permission [133]. Copyright 2018, Elsevier. Wettability, reproduced with permission [143]. Copyright 2019, Elsevier. Water in Salt, reproduced with permission [13]. Copyright 2022, Oxford University Press. Additives, reproduced with permission [154]. Copyright 2022, American Chemical Society. Gel framework, reproduced with permission [189]. Copyright 2018, Wiley-VCH. Photothermal, reproduced with permission [197]. Copyright 2021, Elsevier. Self heating, reproduced with permission [192]. Copyright 2016, Elsevier. External heating, reproduced with permission [193]. Copyright 2013, Elsevier.)

4.1. Electrode design for LTPCs

In the design of electrodes for LTPCs, facilitating ion transport is crucial due to the slower diffusion and transmission of ions at low temperatures. Thus, adopting appropriate strategies for rational structural design becomes imperative. Factors such as conductivity and stability also require careful consideration. It is noteworthy that most pseudocapacitive materials lack excellent properties in all aspects simultaneously. Therefore, a practical approach involves synergistically combining different materials to fabricate composite materials with superior comprehensive properties.

4.2. Electrolyte considerations

Within the realm of LTPCs, the electrolyte's low freezing point and high ionic conductivity are critical parameters directly impacting the electrochemical device performance. These parameters are influenced by various factors such as the type of salt, concentration, viscosity, temperature, and dielectric constant. Our review comprehensively analyzes these influencing factors and summarizes strategies for regulating electrolyte properties. While aqueous, organic, and ionic liquids are current solvents, finding a single solvent with both excellent conductivity and a low melting point poses challenges. Hence, a common approach involves manipulating electrolyte properties by blending different types of solutions to form cosolvents. The emergence of high-entropy electrolyte (HEE) presents a promising choice due to its unique properties. Additionally, the incorporation of a gel network into LTPCs significantly enhances their anti-freezing performance, offering great potential for constructing quasi-solid/state supercapacitors suitable for low-temperature applications. However, each strategy has its limitations, and meeting the needs of low-temperature applications often requires the combination of multiple strategies for LTPC electrolyte development.

4.3. Interface optimization

The interface, serving as the contact surface between electrodes and electrolytes, plays a crucial role in supercapacitor performance by influencing ion diffusion and charge transfer. This role becomes even more vital at low temperatures due to slower interfacial processes such as desolvation and redox reactions. Comprehensive optimization of the entire system is necessary, including optimizing pore structure and surface properties to facilitate electrolyte penetration and wetting, as well as optimizing electrolyte formulations to reduce desolvation energy.

4.4. Thermal-assisted heating strategies

In addition to adjusting the internal low-temperature resistance characteristics of supercapacitors, increasing their actual operating temperature through a thermal-assisted heating strategy has proven effective. This strategy includes both external-assisted heating and self-heating methods. Self-heating strategies encompass designing internal heating circuits, coating surfaces with photothermal materials, and directly utilizing photothermal materials as electrodes. Each strategy has its advantages and limitations, necessitating careful consideration based on specific usage scenarios.

4.5. Challenges and future directions

Despite significant progress in low-temperature supercapacitor development, several challenges persist. Further research is needed to understand the mechanisms of performance degradation and failure at low temperatures, particularly focusing on the electrode/electrolyte interface. This understanding will provide valuable guidance for optimizing electrode and electrolyte materials. Additionally, although various electrode structures have been designed, accurately predicting experimental electrochemical performance remains challenging. Developing a parameter or model that comprehensively considers factors such as specific area, ion accessibility, and space utilization efficiency is essential. Moreover, for electrolyte optimization, current reliance on experimental trial and error methods is inefficient and costly. To address this issue, the development of numerical simulation technology is recommended to accurately predict different electrolyte formulations and ratios, assisting in the advancement of advanced electrolytes. In addition, solid-state electrolytes also are crucial for the advancement of low-temperature supercapacitors, offering inherent stability, safety, and enhanced electrochemical performance compared to traditional liquid electrolytes. Their solid nature eliminates the risk of leakage and evaporation, ensuring reliable operation in harsh environmental conditions where conventional liquid electrolytes may freeze or undergo phase changes. Moreover, solid-state electrolytes facilitate rapid ion transport and charge transfer even in sub-zero temperatures, thus maintaining high-performance energy storage and discharge capabilities. By reducing internal resistance and expanding the operating temperature range, solid-state electrolytes enable supercapacitors to deliver efficient power delivery and faster charging/discharging rates, critical for applications in cold climates or space environments. Additionally, their compatibility with miniaturization and integration allows for the development of compact, lightweight supercapacitor systems suitable for portable electronics, wearables, and space exploration missions, where reliability and performance are paramount. Therefore, the unique properties and potential applications of solid-state electrolytes make them a promising area for future research and development in the field of high-performance supercapacitors for energy storage.

Declaration of competing interest

The authors declare that they have no known competing financial interests or personal relationships that could have appeared to influence the work reported in this paper.

Acknowledgements

Yu Liu acknowledge support by the National Natural Science Foundation of China, under award number No.52202324. This work is also supported by Hundred Talents Program of the Chinese Academy of Sciences. The Chinese Academy of Sciences (CAS) Nanjing Future Energy System Research Institute independently deploys research projects E3550101. We also thanks to Major Basic Research Project for Aircraft Engines and Gas Turbines (No. J2019-II-0008-0028) and Xplorer Prize.

References

[1] Q. Zhu, D. Zhao, M. Cheng, J. Zhou, K.A. Owusu, L. Mai, Y. Yu, A new view of supercapacitors: integrated supercapacitors, Adv. Energy Mater. 9 (36) (2019), https://doi.org/10.1002/aenm.201901081.
[2] S. Chen, S.R. Jeong, S. Tao, Key materials and future perspective for aqueous rechargeable lithium-ion batteries, Materials Rep.: Energy 2 (2) (2022), https://doi.org/10.1016/j.matre.2022.100096.
[3] Y. Liu, Z. Shao, T. Mori, S.P. Jiang, Development of nickel based cermet anode materials in solid oxide fuel cells – now and future, Materials Rep.: Energy 1 (1) (2021), https://doi.org/10.1016/j.matre.2020.11.002.
[4] H. Ren, L. Jia, C. Dang, C. Yang, H. Jia, J. Liu, Experimental investigation on pouch lithium-ion battery thermal management with mini-channels cooling plate based on heat generation characteristic, J. Therm. Sci. 31 (3) (2022) 816–829, https://doi.org/10.1007/s11630-022-1586-9.
[5] Y. Gao, W. Yao, J. Wang, Z. Cui, Thermodynamic analysis of solid oxide fuel cell based combined cooling, heating, and power system integrated with solar-assisted electrolytic cell, J. Therm. Sci. 32 (1) (2023) 93–108, https://doi.org/10.1007/s11630-022-1680-z.
[6] P. Bhojane, Recent advances and fundamentals of Pseudocapacitors: materials, mechanism, and its understanding, J. Energy Storage 45 (2022), https://doi.org/10.1016/j.est.2021.103654.
[7] X. Dong, Y. Yang, B. Wang, Y. Cao, N. Wang, P. Li, Y. Wang, Y. Xia, Low-temperature charge/discharge of rechargeable battery realized by intercalation pseudocapacitive behavior, Adv. Sci. 7 (14) (2020) 2000196, https://doi.org/10.1002/advs.202000196.
[8] C. Huang, S.-X. Zhao, H. Peng, Y.-H. Lin, C.-W. Nan, G.-Z. Cao, Hierarchical porous Li4Ti5O12–TiO2 composite anode materials with pseudocapacitive effect for high-rate and low-temperature applications, J. Mater. Chem. A 6 (29) (2018) 14339–14351, https://doi.org/10.1039/C8TA03172J.
[9] J. Xu, X. Hu, X. Wang, X. Wang, Y. Ju, S. Ge, X. Lu, J. Ding, N. Yuan, Y. Gogotsi, Low-Temperature pseudocapacitive energy storage in Ti3C2T MXene, Energy Storage Mater. 33 (2020) 382–389, https://doi.org/10.1016/j.ensm.2020.08.029.
[10] J. Chen, P.S. Lee, Electrochemical supercapacitors: from mechanism understanding to multifunctional applications, Adv. Energy Mater. 11 (6) (2020), https://doi.org/10.1002/aenm.202003311.
[11] M. Galiński, A. Lewandowski, I. Stępniak, Ionic liquids as electrolytes, Electrochim. Acta 51 (26) (2006) 5567–5580, https://doi.org/10.1016/j.electacta.2006.03.016.
[12] K. Zhu, M. Li, C. Li, X. Xuan, H. Li, Flexible aqueous asymmetric capacitor with SiC-decorated boron-doped graphene cathode and core–shell SiC@graphene anode, Chem. Eng. J. 433 (2022), https://doi.org/10.1016/j.cej.2021.133576.
[13] Y. Zhu, S. Zheng, P. Lu, J. Ma, P. Das, F. Su, H.-M. Cheng, Z.-S. Wu, Kinetic regulation of MXene with water-in-LiCl electrolyte for high-voltage micro-supercapacitors, Natl. Sci. Rev. 9 (7) (2022), https://doi.org/10.1093/nsr/nwac024.
[14] C. Zhong, Y. Deng, W. Hu, J. Qiao, L. Zhang, J. Zhang, A review of electrolyte materials and compositions for electrochemical supercapacitors, Chem. Soc. Rev. 44 (21) (2015) 7484–7539, https://doi.org/10.1039/C5CS00303B.
[15] J.P.A. Santos, M.J. Pinzón, É.A. Santos, R. Vicentini, C.J.B. Pagan, L.M. Da Silva, H. Zanin, Boosting energy-storage capability in carbon-based supercapacitors using low-temperature water-in-salt electrolytes, J. Energy Chem. 70 (2022) 521–530, https://doi.org/10.1016/j.jechem.2022.02.055.
[16] C.-Y. Li, M. Chen, S. Liu, X. Lu, J. Meng, J. Yan, H.D. Abruña, G. Feng, T. Lian, Unconventional interfacial water structure of highly concentrated aqueous electrolytes at negative electrode polarizations, Nat. Commun. 13 (1) (2022) 5330, https://doi.org/10.1038/s41467-022-33129-8.
[17] P.-y. Hung, H. Zhang, H. Lin, Q. Guo, K.-t. Lau, B. Jia, Specializing liquid electrolytes and carbon-based materials in EDLCs for low-temperature applications, J. Energy Chem. 68 (2022) 580–602, https://doi.org/10.1016/j.jechem.2021.12.012.
[18] E.J. Brandon, W.C. West, M.C. Smart, L.D. Whitcanack, G.A. Plett, Extending the low temperature operational limit of double-layer capacitors, J. Power Sources 170 (1) (2007) 225–232, https://doi.org/10.1016/j.jpowsour.2007.04.001.
[19] J. Lang, X. Zhang, L. Liu, B. Yang, J. Yang, X. Yan, Highly enhanced energy density of supercapacitors at extremely low temperatures, J. Power Sources 423 (2019) 271–279, https://doi.org/10.1016/j.jpowsour.2019.03.096.
[20] Y. Liu, S.P. Jiang, Z. Shao, Intercalation pseudocapacitance in electrochemical energy storage: recent advances in fundamental understanding and materials development, Mater. Today Adv. 7 (2020), https://doi.org/10.1016/j.mtadv.2020.100072.
[21] N.R. Chodankar, S.J. Patil, S.K. Hwang, S.V. Karekar, K. Jayaramulu, W. Zhang, D.P. Dubal, Y.S. Huh, Y.-K. Han, Supercapacitors operated at extremely low environmental temperatures, J. Mater. Chem. A 9 (47) (2021) 26603–26627, https://doi.org/10.1039/d1ta08538g.
[22] X. Wang, W. Chen, X. Shi, P. Das, S. Zheng, J. Qin, C. Sun, Z.-S. Wu, Microfluidics-assisted fabrication of all-flexible substrate-free micro-supercapacitors with customizable configuration and high performance, Adv. Energy Mater. 13 (28) (2023) 2203535, https://doi.org/10.1002/aenm.202203535.
[23] J. Xu, N. Yuan, J.M. Razal, Y. Zheng, X. Zhou, J. Ding, K. Cho, S. Ge, R. Zhang, Y. Gogotsi, R.H. Baughman, Temperature-independent capacitance of carbon-based supercapacitor from −100 to 60 °C, Energy Storage Mater. 22 (2019) 323–329, https://doi.org/10.1016/j.ensm.2019.02.016.
[24] Y. Korenblit, A. Kajdos, W.C. West, M.C. Smart, E.J. Brandon, A. Kvit, J. Jagiello, G. Yushin, In situ studies of ion transport in microporous supercapacitor electrodes at ultralow temperatures, Adv. Funct. Mater. 22 (8) (2012) 1655–1662, https://doi.org/10.1002/adfm.201102573.
[25] L. Ma, G. Sun, J. Ran, S. Lv, X. Shen, H. Tong, One-pot template-free strategy toward 3D hierarchical porous nitrogen-doped carbon framework in situ armored homogeneous NiO nanoparticles for high-performance asymmetric supercapacitors, ACS Appl. Mater. Interfaces 10 (26) (2018) 22278–22290, https://doi.org/10.1021/acsami.8b05967.
[26] J. Xu, X. Wang, X. Zhou, N. Yuan, S. Ge, J. Ding, Activated carbon coated CNT core-shell nanocomposite for supercapacitor electrode with excellent rate performance at low temperature, Electrochim. Acta 301 (2019) 478–486, https://doi.org/10.1016/j.electacta.2019.02.021.
[27] J. Liu, X. Li, B. Jin, H. Tang, L. Ma, R. Zhang, J. Ran, H. Zhang, Optimizing porous structure of carbon electrodes for temperature-independent capacitance at sub-zero temperatures, Chem. Eng. J. 441 (2022), https://doi.org/10.1016/j.cej.2022.136053.

[28] J. Yang, H. Wu, M. Zhu, W. Ren, Y. Lin, H. Chen, F. Pan, Optimized mesopores enabling enhanced rate performance in novel ultrahigh surface area meso-/microporous carbon for supercapacitors, Nano Energy 33 (2017) 453–461, https://doi.org/10.1016/j.nanoen.2017.02.007.
[29] V. Pavlenko, S. Kalybekkyzy, D. Knez, Q. Abbas, Z. Mansurov, Z. Bakenov, A. Ng, Revisiting the carbon mesopore contribution towards improved performance of ionic liquid–based EDLCs at sub-zero temperatures, Ionics 28 (2) (2021) 893–901, https://doi.org/10.1007/s11581-021-04354-w.
[30] A.J. Pak, G.S. Hwang, Charging rate dependence of ion migration and stagnation in ionic-liquid-filled carbon nanopores, J. Phys. Chem. C 120 (43) (2016) 24560–24567, https://doi.org/10.1021/acs.jpcc.6b06637.
[31] L. Sun, M.G. Campbell, M. Dinca, Electrically conductive porous metal-organic frameworks, Angew Chem. Int. Ed. Engl. 55 (11) (2016) 3566–3579, https://doi.org/10.1002/anie.201506219.
[32] L.S. Xie, G. Skorupskii, M. Dinca, Electrically conductive metal-organic frameworks, Chem. Rev. 120 (16) (2020) 8536–8580, https://doi.org/10.1021/acs.chemrev.9b00766.
[33] S. Lany, Semiconducting transition metal oxides, J. Phys. Condens. Matter 27 (28) (2015) 283203, https://doi.org/10.1088/0953-8984/27/28/283203.
[34] Y. Yang, S.W. Ng, D. Chen, J. Chang, D. Wang, J. Shang, Q. Huang, Y. Deng, Z. Zheng, Freestanding lamellar porous carbon stacks for low-temperature-foldable supercapacitors, Small 15 (48) (2019) e1902071, https://doi.org/10.1002/smll.201902071.
[35] N.R. Chodankar, P.A. Shinde, S.J. Patil, S.-K. Hwang, G.S.R. Raju, K.S. Ranjith, D.P. Dubal, Y.S. Huh, Y.-K. Han, Solution-free self-assembled growth of ordered tricopper phosphide for efficient and stable hybrid supercapacitor, Energy Storage Mater. 39 (2021) 194–202, https://doi.org/10.1016/j.ensm.2021.04.023.
[36] B. Pal, S. Yang, S. Ramesh, V. Thangadurai, R. Jose, Electrolyte selection for supercapacitive devices: a critical review, Nanoscale Adv. 1 (10) (2019) 3807–3835, https://doi.org/10.1039/c9na00374f.
[37] D. Wu, H.J. Feng, L.H. Xu, W.Y. Zhang, Z.J. Zhang, X.Y. Chen, P. Cui, Optimal design of a small-molecule crowding electrolyte and molecular dynamics simulation of an electrode-electrolyte interface for aqueous supercapacitors with a wide operating temperature range, ACS Appl. Energy Mater. 5 (1) (2022) 355–366, https://doi.org/10.1021/acsaem.1c02889.
[38] J.H. Park, N.R. Aluru, Temperature-dependent wettability on a titanium dioxide surface, Mol. Simulat. 35 (1–2) (2009) 31–37, https://doi.org/10.1080/08927020802398884.
[39] X. Gao, X. Du, T.S. Mathis, M. Zhang, X. Wang, J. Shui, Y. Gogotsi, M. Xu, Maximizing ion accessibility in MXene-knotted carbon nanotube composite electrodes for high-rate electrochemical energy storage, Nat. Commun. 11 (1) (2020), https://doi.org/10.1038/s41467-020-19992-3.
[40] L. Jiang, D. Dong, Y.-C. Lu, Design strategies for low temperature aqueous electrolytes, Nano Res. Energy. 1 (2022), https://doi.org/10.26599/nre.2022.9120003.
[41] J.C. Cheftel, J. Lévy, E. Dumay, Pressure-assisted freezing and thawing: principles and potential applications, Food Rev. Int. 16 (4) (2000) 453–483, https://doi.org/10.1081/fri-100102319.
[42] A.D. Buckingham, J.E. Del Bene, S.A.C. McDowell, The hydrogen bond, Chem. Phys. Lett. 463 (1) (2008) 1–10, https://doi.org/10.1016/j.cplett.2008.06.060.
[43] Q. Zhang, Y. Ma, Y. Lu, L. Li, F. Wan, K. Zhang, J. Chen, Modulating electrolyte structure for ultralow temperature aqueous zinc batteries, Nat. Commun. 11 (1) (2020) 4463, https://doi.org/10.1038/s41467-020-18284-0.
[44] M. Matsumoto, S. Saito, I. Ohmine, Molecular dynamics simulation of the ice nucleation and growth process leading to water freezing, Nature 416 (6879) (2002) 409–413, https://doi.org/10.1038/416409a.
[45] Y. Zhang, Y. Sun, J. Nan, F. Yang, Z. Wang, Y. Li, C. Wang, F. Chu, Y. Liu, C. Wang, In situ polymerization of hydrogel electrolyte on electrodes enabling the flexible all-hydrogel supercapacitors with low-temperature adaptability, Small 20 (22) (2024) e2309900, https://doi.org/10.1002/smll.202309900.
[46] T. Zhao, D. Yang, B.-X. Li, Y. Shi, Q. Quan, N. Koratkar, Z.-Z. Yu, A supercapacitor architecture for extreme low-temperature operation featuring MXene/carbon nanotube electrodes with vertically aligned channels and a novel freeze-resistant electrolyte, Adv. Funct. Mater. 34 (24) (2024) 2314825, https://doi.org/10.1002/adfm.202314825.
[47] M. Armand, F. Endres, D.R. MacFarlane, H. Ohno, B. Scrosati, Ionic-liquid materials for the electrochemical challenges of the future, Nat. Mater. 8 (8) (2009) 621–629, https://doi.org/10.1038/nmat2448.
[48] J. Owen, 21 - ionic conductivity, in: G. Allen, J.C. Bevington (Eds.), Comprehensive Polymer Science and Supplements, Pergamon, Amsterdam, 1989, pp. 669–686, https://doi.org/10.1016/B978-0-08-096701-1.00058-6.
[49] E.M. Layton Jr., Modern electrochemistry (bockris, john O'M.; reddy, amulya K. N.), J. Chem. Educ. 52 (1) (1975) A60, https://doi.org/10.1021/ed052pA60.2.
[50] Q. Dou, S. Lei, D.-W. Wang, Q. Zhang, D. Xiao, H. Guo, A. Wang, H. Yang, Y. Li, S. Shi, X. Yan, Safe and high-rate supercapacitors based on an "acetonitrile/water in salt" hybrid electrolyte, Energy Environ. Sci. 11 (11) (2018) 3212–3219, https://doi.org/10.1039/c8ee01040d.
[51] Y. Sun, Y. Wang, L. Liu, B. Liu, Q. Zhang, D. Wu, H. Zhang, X. Yan, Towards the understanding of acetonitrile suppressing salt precipitation mechanism in a water-in-salt electrolyte for low-temperature supercapacitors, J. Mater. Chem. A 8 (35) (2020) 17998–18006, https://doi.org/10.1039/d0ta04538a.
[52] G. Kamath, R.W. Cutler, S.A. Deshmukh, M. Shakourian-Fard, R. Parrish, J. Huether, D.P. Butt, H. Xiong, S.K.R.S. Sankaranarayanan, In silico based rank-order determination and experiments on nonaqueous electrolytes for sodium ion battery applications, J. Phys. Chem. C 118 (25) (2014) 13406–13416, https://doi.org/10.1021/jp502319p.
[53] N. Yao, L. Yu, Z.H. Fu, X. Shen, T.Z. Hou, X. Liu, Y.C. Gao, R. Zhang, C.Z. Zhao, X. Chen, Q. Zhang, Probing the origin of viscosity of liquid electrolytes for lithium batteries, Angew. Chem. Int. Ed. 62 (41) (2023), https://doi.org/10.1002/anie.202305331.
[54] H. Che, S. Chen, Y. Xie, H. Wang, K. Amine, X.-Z. Liao, Z.-F. Ma, Electrolyte design strategies and research progress for room-temperature sodium-ion batteries, Energy Environ. Sci. 10 (5) (2017) 1075–1101, https://doi.org/10.1039/c7ee00524e.
[55] N. Yao, X. Chen, X. Shen, R. Zhang, Z.H. Fu, X.X. Ma, X.Q. Zhang, B.Q. Li, Q. Zhang, An atomic insight into the chemical origin and variation of the dielectric constant in liquid electrolytes, Angew Chem. Int. Ed. Engl. 60 (39) (2021) 21473–21478, https://doi.org/10.1002/anie.202107657.
[56] K.-H. Shen, L.M. Hall, Effects of ion size and dielectric constant on ion transport and transference number in polymer electrolytes, Macromolecules 53 (22) (2020) 10086–10096, https://doi.org/10.1021/acs.macromol.0c02161.
[57] X. Jiang, H. Zhang, Y. Qu, Z. Wang, Y. Xie, W. Zhang, H. Hu, Z. He, Engineering electrolyte strong-weak coupling effect toward wide-temperature supercapacitor, Energy Storage Mater. 68 (2024) 103374, https://doi.org/10.1016/j.ensm.2024.103374.
[58] J. Zhu, Y. Xu, J. Wang, J. Lin, X. Sun, S. Mao, The effect of various electrolyte cations on electrochemical performance of polypyrrole/RGO based supercapacitors, Phys. Chem. Chem. Phys. 17 (43) (2015) 28666–28673, https://doi.org/10.1039/c5cp04080a.
[59] E.R. Nightingale Jr., Phenomenological theory of ion solvation. Effective radii of hydrated ions, J. Phys. Chem. 63 (9) (1959) 1381–1387, https://doi.org/10.1021/j150579a011.
[60] P.W. Atkins, J. De Paula, J. Keeler, Atkins' Physical Chemistry, Oxford university press, 2023.
[61] O. Tanaike, H. Hatori, Y. Yamada, S. Shiraishi, A. Oya, Preparation and pore control of highly mesoporous carbon from defluorinated PTFE, Carbon 41 (9) (2003) 1759–1764, https://doi.org/10.1016/S0008-6223(03)00146-5.
[62] B. Yao, H. Peng, H. Zhang, J. Kang, C. Zhu, G. Delgado, D. Byrne, S. Faulkner, M. Freyman, X. Lu, M.A. Worsley, J.Q. Lu, Y. Li, Printing porous carbon aerogels for low temperature supercapacitors, Nano Lett. 21 (9) (2021) 3731–3737, https://doi.org/10.1021/acs.nanolett.0c04780.
[63] N.C. Abeykoon, J.S. Bonso, J.P. Ferraris, Supercapacitor performance of carbon nanofiber electrodes derived from immiscible PAN/PMMA polymer blends, RSC Adv. 5 (26) (2015) 19865–19873, https://doi.org/10.1039/c4ra16594b.
[64] Q. Zhang, Y. Li, J. Zhu, L. Lan, C. Li, J. Mao, F. Wang, Z. Zhang, L. Wang, Ultra-low temperature flexible supercapacitor based on hierarchically structured pristine polypyrrole membranes, Chem. Eng. J. 420 (2021), https://doi.org/10.1016/j.cej.2021.129712.
[65] V. Subramanian, S.C. Hall, P.H. Smith, B. Rambabu, Mesoporous anhydrous RuO2 as a supercapacitor electrode material, Solid State Ionics 175 (1) (2004) 511–515, https://doi.org/10.1016/j.ssi.2004.01.070.
[66] Y. Liu, Z. Wang, Y. Zhong, M. Tade, W. Zhou, Z. Shao, Molecular design of mesoporous NiCo2O4 and NiCo2S4 with sub-micrometer-polyhedron architectures for efficient pseudocapacitive energy storage, Adv. Funct. Mater. 27 (28) (2017) 1701229, https://doi.org/10.1002/adfm.201701229.
[67] Y. Wang, J. Guo, T. Wang, J. Shao, D. Wang, Y.-W. Yang, Mesoporous transition metal oxides for supercapacitors, Nanomaterials 5 (4) (2015) 1667–1689, https://doi.org/10.3390/nano5041667.
[68] K. Luo, Q. Zheng, Y. Yu, C. Wang, S. Jiang, H. Zhang, Y. Liu, Y. Guo, Urea-assisted sol-gel synthesis of LaMnO3 perovskite with accelerated catalytic activity for application in Zn-air battery, Batteries 9 (2) (2023), https://doi.org/10.3390/batteries9020090.
[69] Y. Liu, X. Xu, Z. Shao, S.P. Jiang, Metal-organic frameworks derived porous carbon, metal oxides and metal sulfides-based compounds for supercapacitors application, Energy Storage Mater. 26 (2020) 1–22, https://doi.org/10.1016/j.ensm.2019.12.019.
[70] X.B. Chen, J.P. Issi, M. Cassart, J. Devaux, D. Billaud, Temperature dependence of the conductivity in conducting polymer composites, Polymer 35 (24) (1994) 5256–5258, https://doi.org/10.1016/0032-3861(94)90477-4.
[71] J.N. Tiwari, R.N. Tiwari, K.S. Kim, Zero-dimensional, one-dimensional, two-dimensional and three-dimensional nanostructured materials for advanced electrochemical energy devices, Prog. Mater. Sci. 57 (4) (2012) 724–803, https://doi.org/10.1016/j.pmatsci.2011.08.003.
[72] A. Devadas, S. Baranton, T.W. Napporn, C. Coutanceau, Tailoring of RuO2 nanoparticles by microwave assisted "Instant method" for energy storage applications, J. Power Sources 196 (8) (2011) 4044–4053, https://doi.org/10.1016/j.jpowsour.2010.11.149.
[73] B. Ding, X. Wu, Transition metal oxides anchored on graphene/carbon nanotubes conductive network as both the negative and positive electrodes for asymmetric supercapacitor, J. Alloys Compd. 842 (2020), https://doi.org/10.1016/j.jallcom.2020.155838.
[74] X. Liu, P.G. Pickup, Performance and low temperature behaviour of hydrous ruthenium oxide supercapacitors with improved power densities, Energy Environ. Sci. (2008), https://doi.org/10.1039/b809939a.
[75] Y. Ma, X. Xie, W. Yang, Z. Yu, X. Sun, Y. Zhang, X. Yang, H. Kimura, C. Hou, Z. Guo, W. Du, Recent advances in transition metal oxides with different dimensions as electrodes for high-performance supercapacitors, Adv. Compos. Hybrid Mater. 4 (4) (2021) 906–924, https://doi.org/10.1007/s42114-021-00358-2.
[76] W. Wei, W. Chen, L. Mi, J. Xu, J. Zhang, High-rate performance aqueous-based supercapacitors at −30 °C driven by novel 1D Ni(OH)2 nanorods and a two-solute

electrolyte, J. Mater. Chem. A 9 (42) (2021) 23860–23872, https://doi.org/10.1039/d1ta07412a.
[77] J. Zhang, N. Kong, S. Uzun, A. Levitt, S. Seyedin, P.A. Lynch, S. Qin, M. Han, W. Yang, J. Liu, X. Wang, Y. Gogotsi, J.M. Razal, Scalable manufacturing of free-standing, strong Ti3C2Tx MXene films with outstanding conductivity, Adv. Mater. 32 (23) (2020), https://doi.org/10.1002/adma.202001093.
[78] M.R. Lukatskaya, O. Mashtalir, C.E. Ren, Y. Dall'Agnese, P. Rozier, P.L. Taberna, M. Naguib, P. Simon, M.W. Barsoum, Y. Gogotsi, Cation intercalation and high volumetric capacitance of two-dimensional titanium carbide, Science 341 (6153) (2013) 1502–1505, https://doi.org/10.1126/science.1241488.
[79] X. Xu, L. Yang, W. Zheng, H. Zhang, F. Wu, Z. Tian, P. Zhang, Z. Sun, MXenes with applications in supercapacitors and secondary batteries: a comprehensive review, Materials Rep.: Energy 2 (1) (2022), https://doi.org/10.1016/j.matre.2022.100080.
[80] Y. Chang, B. Wang, Y. Huo, K. Zhai, L. Liu, P. Li, A. Nie, C. Mu, J. Xiang, Z. Zhao, F. Wen, Z. Liu, Y. Tian, Layered porous materials indium triphosphide InP3 for high-performance flexible all-solid-state supercapacitors, J. Power Sources 438 (2019), https://doi.org/10.1016/j.jpowsour.2019.227010.
[81] X. Wu, R. Liu, J. Zhao, Z. Fan, Advanced carbon materials with different spatial dimensions for supercapacitors, Nano Mater. Sci. 3 (3) (2021) 241–267, https://doi.org/10.1016/j.nanoms.2021.01.002.
[82] B. Anasori, M.R. Lukatskaya, Y. Gogotsi, 2D metal carbides and nitrides (MXenes) for energy storage, Nat. Rev. Mater. 2 (2) (2017), https://doi.org/10.1038/natrevmats.2016.98.
[83] J. Yin, K. Wei, J. Zhang, S. Liu, X. Wang, X. Wang, Q. Zhang, Z. Qin, T. Jiao, MXene-based film electrode and all-round hydrogel electrolyte for flexible all-solid supercapacitor with extremely low working temperature, Cell Rep. Phy. Sci. 3 (5) (2022), https://doi.org/10.1016/j.xcrp.2022.100893.
[84] L. Sun, Q. Fu, C. Pan, Mn3O4 embedded 3D multi-heteroatom codoped carbon sheets/carbon foams composites for high-performance flexible supercapacitors, J. Alloys Compd. 849 (2020), https://doi.org/10.1016/j.jallcom.2020.156666.
[85] W.-Y. Tsai, R. Lin, S. Murali, L. Li Zhang, J.K. McDonough, R.S. Ruoff, P.-L. Taberna, Y. Gogotsi, P. Simon, Outstanding performance of activated graphene based supercapacitors in ionic liquid electrolyte from −50 to 80°C, Nano Energy 2 (3) (2013) 403–411, https://doi.org/10.1016/j.nanoen.2012.11.006.
[86] F. Yang, D. Hegh, D. Song, J. Zhang, K.A.S. Usman, C. Liu, Z. Wang, W. Ma, W. Yang, S. Qin, J.M. Razal, Synthesis of nitrogen-sulfur co-doped Ti3C2T MXene with enhanced electrochemical properties, Materials Rep.: Energy 2 (1) (2022), https://doi.org/10.1016/j.matre.2022.100079.
[87] C. Chen, D. Yu, G. Zhao, B. Du, W. Tang, L. Sun, Y. Sun, F. Besenbacher, M. Yu, Three-dimensional scaffolding framework of porous carbon nanosheets derived from plant wastes for high-performance supercapacitors, Nano Energy 27 (2016) 377–389, https://doi.org/10.1016/j.nanoen.2016.07.020.
[88] Z. Bi, Q. Kong, Y. Cao, G. Sun, F. Su, X. Wei, X. Li, A. Ahmad, L. Xie, C.-M. Chen, Biomass-derived porous carbon materials with different dimensions for supercapacitor electrodes: a review, J. Mater. Chem. A 7 (27) (2019) 16028–16045, https://doi.org/10.1039/c9ta04436a.
[89] Y. Qiu, Z. Wang, M. Jin, J. Chen, C. Miao, S. Zhang, L. Lai, Amorphous carbon interweaved mesoporous all-carbon electrode for wide-temperature range supercapacitors, Electrochim. Acta 424 (2022), https://doi.org/10.1016/j.electacta.2022.140622.
[90] K. Qin, J. Baucom, L. Diao, Y. Lu, N. Zhao, Compacted N-doped 3D bicontinuous nanoporous graphene/carbon nanotubes@Ni-doped MnO2 electrode for ultrahigh volumetric performance all-solid-state supercapacitors at wide temperature range, Small 18 (33) (2022), https://doi.org/10.1002/smll.202203166.
[91] Q. Wang, J. Yan, Z. Fan, Carbon materials for high volumetric performance supercapacitors: design, progress, challenges and opportunities, Energy Environ. Sci. 9 (3) (2016) 729–762, https://doi.org/10.1039/C5EE03109E.
[92] M. Zhang, T. Xu, D. Wang, T. Yao, Z. Xu, Q. Liu, L. Shen, Y. Yu, A 3D-printed proton pseudocapacitor with ultrahigh mass loading and areal energy density for fast energy storage at low temperature, Adv. Mater. (2023) e2209963, https://doi.org/10.1002/adma.202209963.
[93] K. Li, J. Zhao, A. Zhussupbekova, C.E. Shuck, L. Hughes, Y. Dong, S. Barwich, S. Vaesen, I.V. Shvets, M. Mobius, W. Schmitt, Y. Gogotsi, V. Nicolosi, 4D printing of MXene hydrogels for high-efficiency pseudocapacitive energy storage, Nat. Commun. 13 (1) (2022) 6884, https://doi.org/10.1038/s41467-022-34583-0.
[94] X. Li, Y. Wu, D. Yan, M. Xie, S. Zhang, C. Deng, "Bubble-in-bowl" structured metal phosphide@N, P codoped carbon via bio-assisted combustion synthesis for high-performance potassium-ion hybrid capacitors in a wide temperature range, J. Mater. Chem. A 9 (29) (2021) 16028–16038, https://doi.org/10.1039/d1ta04625j.
[95] D. Zhu, J. Jiang, D. Sun, X. Qian, Y. Wang, L. Li, Z. Wang, X. Chai, L. Gan, M. Liu, A general strategy to synthesize high-level N-doped porous carbons via Schiff-base chemistry for supercapacitors, J. Mater. Chem. A 6 (26) (2018) 12334–12343, https://doi.org/10.1039/c8ta02341g.
[96] X. Ma, G. Ning, Y. Kan, Y. Ma, C. Qi, B. Chen, Y. Li, X. Lan, J. Gao, Synthesis of S-doped mesoporous carbon fibres with ultrahigh S concentration and their application as high performance electrodes in supercapacitors, Electrochim. Acta 150 (2014) 108–113, https://doi.org/10.1016/j.electacta.2014.10.128.
[97] R. Vellacheri, A. Al-Haddad, H. Zhao, W. Wang, C. Wang, Y. Lei, High performance supercapacitor for efficient energy storage under extreme environmental temperatures, Nano Energy 8 (2014) 231–237, https://doi.org/10.1016/j.nanoen.2014.06.015.
[98] C. Chen, Z. Li, Y. Xu, S. Li, L. Wu, D. Xiao, H. Dou, X. Zhang, Tailored hierarchical porous carbon through template modification for antifreezing quasi-solid-state zinc ion hybrid supercapacitors, Adv. Energy Sustain. Res. 2 (6) (2021), https://doi.org/10.1002/aesr.202000112.
[99] Y. Shang, C. Wang, X. He, J. Li, Q. Peng, E. Shi, R. Wang, S. Du, A. Cao, Y. Li, Self-stretchable, helical carbon nanotube yarn supercapacitors with stable performance under extreme deformation conditions, Nano Energy 12 (2015) 401–409, https://doi.org/10.1016/j.nanoen.2014.11.048.
[100] Z.H. Huang, T.Y. Liu, Y. Song, Y. Li, X.X. Liu, Balancing the electrical double layer capacitance and pseudocapacitance of hetero-atom doped carbon, Nanoscale 9 (35) (2017) 13119–13127, https://doi.org/10.1039/c7nr04234e.
[101] J.P. Paraknowitsch, A. Thomas, Doping carbons beyond nitrogen: an overview of advanced heteroatom doped carbons with boron, sulphur and phosphorus for energy applications, Energy Environ. Sci. 6 (10) (2013) 2839–2855, https://doi.org/10.1039/C3EE41444B.
[102] Q. Li, C. Lu, D. Xiao, H. Zhang, C. Chen, L. Xie, Y. Liu, S. Yuan, Q. Kong, K. Zheng, J. Yin, β-Ni(OH)2 nanosheet arrays grown on biomass-derived hollow carbon microtubes for high-performance asymmetric supercapacitors, Chemelectrochem 5 (9) (2018) 1279–1287, https://doi.org/10.1002/celc.201800024.
[103] Y. Zhang, L. Xie, S. Li, Z. Hu, Fabrication of multi-purposed supercapacitors based on N-doped porous carbon framework, Results in Chemistry 4 (2022), https://doi.org/10.1016/j.rechem.2022.100479.
[104] S. Zhang, A. Ikoma, K. Ueno, Z. Chen, K. Dokko, M. Watanabe, Protic-salt-derived nitrogen/sulfur-codoped mesoporous carbon for the oxygen reduction reaction and supercapacitors, ChemSusChem 8 (9) (2015) 1608–1617, https://doi.org/10.1002/cssc.201403320.
[105] N. Zhang, F. Liu, S.-D. Xu, F.-Y. Wang, Q. Yu, L. Liu, Nitrogen–phosphorus co-doped hollow carbon microspheres with hierarchical micro–meso–macroporous shells as efficient electrodes for supercapacitors, J. Mater. Chem. A 5 (43) (2017) 22631–22640, https://doi.org/10.1039/C7TA07488C.
[106] L. Sun, Y. Yao, Y. Zhou, L. Li, H. Zhou, M. Guo, S. Liu, C. Feng, Z. Qi, B. Gao, Solvent-free synthesis of N/S-codoped hierarchically porous carbon materials from protic ionic liquids for temperature-resistant, flexible supercapacitors, ACS Sustain. Chem. Eng. 6 (10) (2018) 13494–13503, https://doi.org/10.1021/acssuschemeng.8b03528.
[107] Y. Liu, W. Wang, X. Xu, J.-P. Marcel Veder, Z. Shao, Recent advances in anion-doped metal oxides for catalytic applications, J. Mater. Chem. A 7 (13) (2019) 7280–7300, https://doi.org/10.1039/c8ta09913h.
[108] T. Li, J. Wu, X. Xiao, B. Zhang, Z. Hu, J. Zhou, P. Yang, X. Chen, B. Wang, L. Huang, Band gap engineering of MnO2 through in situ Al-doping for applicable pseudocapacitors, RSC Adv. 6 (17) (2016) 13914–13919, https://doi.org/10.1039/c5ra26830c.
[109] J. Cherusseri, K.K. Kar, Hierarchical carbon nanopetal/polypyrrole nanocomposite electrodes with brush-like architecture for supercapacitors, Phys. Chem. Chem. Phys. 18 (12) (2016) 8587–8597, https://doi.org/10.1039/C6CP00150E.
[110] B. Liu, D. Kong, J. Zhang, Y. Wang, T. Chen, C. Cheng, H.Y. Yang, 3D hierarchical Co3O4@Co3S4 nanoarrays as cathode materials for asymmetric pseudocapacitors, J. Mater. Chem. A 4 (9) (2016) 3287–3296, https://doi.org/10.1039/c5ta09344a.
[111] J. Li, W. Zhao, F. Huang, A. Manivannan, N. Wu, Single-crystalline Ni(OH)2 and NiO nanoplatelet arrays as supercapacitor electrodes, Nanoscale 3 (12) (2011) 5103–5109, https://doi.org/10.1039/C1NR10802F.
[112] Y. Liu, Z.-Y. Liu, H. Zhang, Y. Xu, H. Chen, Efficient and stable anode material for Li batteries: utilizing Co3O4 nanoparticles modified active graphite derived from date pulp, Energy Fuels 37 (11) (2023) 7982–7989, https://doi.org/10.1021/acs.energyfuels.3c00528.
[113] Y. Liu, Z. Wang, Y. Zhong, X. Xu, J.-P.M. Veder, M.R. Rowles, M. Saunders, R. Ran, Z. Shao, Activation-free supercapacitor electrode based on surface-modified Sr2CoMo1-xNixO6-δ perovskite, Chem. Eng. J. 390 (2020), https://doi.org/10.1016/j.cej.2020.124645.
[114] X. Zhang, X. Liu, Y. Zeng, Y. Tong, X. Lu, Oxygen defects in promoting the electrochemical performance of metal oxides for supercapacitors: recent advances and challenges, Small Methods 4 (6) (2020), https://doi.org/10.1002/smtd.201900823.
[115] X. Chang, T. Liu, W. Li, M. He, Z. Ren, J. Bai, Dual modulation of the morphology and electric conductivity of NiCoP on nickel foam by Fe doping as a superior stability electrode for high energy supercapacitors, Nanoscale 13 (41) (2021) 17442–17456, https://doi.org/10.1039/d1nr04783c.
[116] X. Wei, H. Wu, L. Li, 3D N-doped carbon continuous network supported P-doped ZnCo2O4 nanosheets with rich oxygen vacancies for high-performance asymmetric pseudocapacitor, J. Alloys Compd. 861 (2021), https://doi.org/10.1016/j.jallcom.2020.158544.
[117] Y. Liu, Z. Wang, J.-P.M. Veder, Z. Xu, Y. Zhong, W. Zhou, M.O. Tade, S. Wang, Z. Shao, Highly defective layered double perovskite oxide for efficient energy storage via reversible pseudocapacitive oxygen-anion intercalation, Adv. Energy Mater. 8 (11) (2018) 1702604, https://doi.org/10.1002/aenm.201702604.
[118] Q.-L. Wu, S.-X. Zhao, L. Yu, X.-X. Zheng, Y.-F. Wang, L.-Q. Yu, C.-W. Nan, G. Cao, Oxygen vacancy-enriched MoO3−x nanobelts for asymmetric supercapacitors with excellent room/low temperature performance, J. Mater. Chem. A 7 (21) (2019) 13205–13214, https://doi.org/10.1039/c9ta03471d.
[119] X. Guan, J. Chen, E. Zhu, P. Yin, L. Yang, X. Guan, G. Wang, Intrinsic electrochemical activity modulation of MOF-derived C/N-NiCoMn-LDH/Ag electrode for low temperature hybrid supercapacitors, J. Mater. Sci. Technol. 150 (2023) 145–158, https://doi.org/10.1016/j.jmst.2022.11.036.
[120] Y. Zhong, X. Xia, F. Shi, J. Zhan, J. Tu, H.J. Fan, Transition metal carbides and nitrides in energy storage and conversion, Adv. Sci. 3 (5) (2016), https://doi.org/10.1002/advs.201500286.

[121] Q. Luo, C. Lu, L. Liu, M. Zhu, A review on the synthesis of transition metal nitride nanostructures and their energy related applications, Green Energy Environ. 8 (2) (2023) 406–437, https://doi.org/10.1016/j.gee.2022.07.002.
[122] X. Geng, Y. Zhang, Y. Han, J. Li, L. Yang, M. Benamara, L. Chen, H. Zhu, Two-dimensional water-coupled metallic MoS2 with nanochannels for ultrafast supercapacitors, Nano Lett. 17 (3) (2017) 1825–1832, https://doi.org/10.1021/acs.nanolett.6b05134.
[123] W. Liu, F. Zhu, Y. Liu, W. Shi, Hierarchical CoP@Ni(OH)2·0.75H2O core-shell nanosheet arrays on carbon cloth for high-performance supercapacitors, J. Colloid Interface Sci. 578 (2020) 1–9, https://doi.org/10.1016/j.jcis.2020.05.107.
[124] J. Jiang, Z. Li, X. He, Y. Hu, F. Li, P. Huang, C. Wang, Novel skutterudite CoP3–based asymmetric supercapacitor with super high energy density, Small 16 (31) (2020) 2000180, https://doi.org/10.1002/smll.202000180.
[125] X. Xia, J. Zhan, Y. Zhong, X. Wang, J. Tu, H.J. Fan, Single-Crystalline, metallic TiC nanowires for highly robust and wide-temperature electrochemical energy storage, Small 13 (5) (2017), https://doi.org/10.1002/smll.201602742.
[126] Y. Huang, H. Li, Z. Wang, M. Zhu, Z. Pei, Q. Xue, Y. Huang, C. Zhi, Nanostructured Polypyrrole as a flexible electrode material of supercapacitor, Nano Energy 22 (2016) 422–438, https://doi.org/10.1016/j.nanoen.2016.02.047.
[127] Y. Yin, Z. Fang, J. Chen, Y. Peng, L. Zhu, C. Wang, Y. Wang, X. Dong, Y. Xia, Hybrid Li-ion capacitor operated within an all-climate temperature range from-60 to+55 degrees C, ACS Appl. Mater. Interfaces 13 (38) (2021) 45630–45638, https://doi.org/10.1021/acsami.1c14308.
[128] J. Kong, G. Xiong, Z. Bo, X. Lu, K. Yi, W. Kuang, S. Yang, H. Yang, S. Tian, J. Yan, K. Cen, Well-aligned hierarchical graphene-based electrodes for pseudocapacitors with outstanding low-temperature stability, Chemelectrochem 6 (10) (2019) 2788–2795, https://doi.org/10.1002/celc.201900601.
[129] L. Tang, Y. Wang, Y. Li, H. Feng, J. Lu, J. Li, Preparation, structure, and electrochemical properties of reduced graphene sheet films, Adv. Funct. Mater. 19 (17) (2009) 2782–2789, https://doi.org/10.1002/adfm.200900377.
[130] Y.-T. Weng, H.-A. Pan, N.-L. Wu, G.Z. Chen, Titanium carbide nanocube core induced interfacial growth of crystalline polypyrrole/polyvinyl alcohol lamellar shell for wide-temperature range supercapacitors, J. Power Sources 274 (2015) 1118–1125, https://doi.org/10.1016/j.jpowsour.2014.10.158.
[131] F.M. Guo, R.Q. Xu, X. Cui, L. Zhang, K.L. Wang, Y.W. Yao, J.Q. Wei, High performance of stretchable carbon nanotube–polypyrrole fiber supercapacitors under dynamic deformation and temperature variation, J. Mater. Chem. A 4 (23) (2016) 9311–9318, https://doi.org/10.1039/c6ta02437h.
[132] X. Wu, L. Meng, Q. Wang, W. Zhang, Y. Wang, Outstanding performance supercapacitor based on the ternary graphene-silver-polypyrrole hybrid nanocomposite from −45 to 80 °C, Mater. Chem. Phys. 206 (2018) 259–269, https://doi.org/10.1016/j.matchemphys.2017.12.028.
[133] Z. Wang, J. Cheng, J. Zhou, J. Zhang, H. Huang, J. Yang, Y. Li, B. Wang, All-climate aqueous fiber-shaped supercapacitors with record areal energy density and high safety, Nano Energy 50 (2018) 106–117, https://doi.org/10.1016/j.nanoen.2018.05.029.
[134] M. Toupin, D. Bélanger, I.R. Hill, D. Quinn, Performance of experimental carbon blacks in aqueous supercapacitors, J. Power Sources 140 (1) (2005) 203–210, https://doi.org/10.1016/j.jpowsour.2004.08.014.
[135] K. Xu, A. von Cresce, U. Lee, Differentiating contributions to "ion transfer" barrier from interphasial resistance and Li+ desolvation at electrolyte/graphite interface, Langmuir 26 (13) (2010) 11538–11543, https://doi.org/10.1021/la1009994.
[136] J. Xu, X. Wang, N. Yuan, J. Ding, S. Qin, J.M. Razal, X. Wang, S. Ge, Y. Gogotsi, Extending the low temperature operational limit of Li-ion battery to −80 °C, Energy Storage Mater. 23 (2019) 383–389, https://doi.org/10.1016/j.ensm.2019.04.033.
[137] D. Hubble, D.E. Brown, Y. Zhao, C. Fang, J. Lau, B.D. McCloskey, G. Liu, Liquid electrolyte development for low-temperature lithium-ion batteries, Energy Environ. Sci. 15 (2) (2022) 550–578, https://doi.org/10.1039/d1ee01789f.
[138] V.D. Nithya, R. Kalai Selvan, D. Kalpana, L. Vasylechko, C. Sanjeeviraja, Synthesis of Bi2WO6 nanoparticles and its electrochemical properties in different electrolytes for pseudocapacitor electrodes, Electrochim. Acta 109 (2013) 720–731, https://doi.org/10.1016/j.electacta.2013.07.138.
[139] J.H. Chae, G.Z. Chen, Influences of ions and temperature on performance of carbon nano-particulates in supercapacitors with neutral aqueous electrolytes, Particuology 15 (2014) 9–17, https://doi.org/10.1016/j.partic.2013.02.008.
[140] D. Lu, R. Li, M.M. Rahman, P. Yu, L. Lv, S. Yang, Y. Huang, C. Sun, S. Zhang, H. Zhang, J. Zhang, X. Xiao, T. Deng, L. Fan, L. Chen, J. Wang, E. Hu, C. Wang, X. Fan, Ligand-channel-enabled ultrafast Li-ion conduction, Nature 627 (8002) (2024) 101–107, https://doi.org/10.1038/s41586-024-07045-4.
[141] X. Chen, Z. Li, H. Zhao, J. Li, W. Li, C. Han, Y. Zhang, L. Lu, J. Li, X. Qiu, Dominant solvent-separated ion pairs in electrolytes enable superhigh conductivity for fast-charging and low-temperature lithium ion batteries, ACS Nano (2024), https://doi.org/10.1021/acsnano.3c12877.
[142] X. Shi, L. Sun, X. Zhang, J. Qian, J. Hu, F. Xie, H. Zhang, Y. Zhang, Application of NiCoP/NiCo2N designed by heterogeneous interface engineering in low-temperature flexible supercapacitors, J. Energy Storage 54 (2022), https://doi.org/10.1016/j.est.2022.105302.
[143] T. Liu, K. Wang, Y. Chen, S. Zhao, Y. Han, Dominant role of wettability in improving the specific capacitance, Green Energy Environ. 4 (2) (2019) 171–179, https://doi.org/10.1016/j.gee.2019.01.010.
[144] M. Li, Y. Ding, Y. Sun, Y. Ren, J. Yang, B. Yin, H. Li, S. Zhang, T. Ma, Emerging rechargeable aqueous magnesium ion battery, Materials Rep.: Energy 2 (4) (2022), https://doi.org/10.1016/j.matre.2022.100161.
[145] M. Salanne, Ionic liquids for supercapacitor applications, Top. Curr. Chem. 375 (3) (2017) 63, https://doi.org/10.1007/s41061-017-0150-7.
[146] C. You, W. Fan, X. Xiong, H. Yang, L. Fu, T. Wang, F. Wang, Z. Zhu, J. He, Y. Wu, Design strategies for anti-freeze electrolytes in aqueous energy storage devices at low temperatures, Adv. Funct. Mater. (2024), https://doi.org/10.1002/adfm.202403616.
[147] S.-W. Xu, M.-C. Zhang, G.-Q. Zhang, J.-H. Liu, X.-Z. Liu, X. Zhang, D.-D. Zhao, C.-L. Xu, Y.-Q. Zhao, Temperature-dependent performance of carbon-based supercapacitors with water-in-salt electrolyte, J. Power Sources 441 (2019), https://doi.org/10.1016/j.jpowsour.2019.227220.
[148] J. Yin, L. Qi, H. Wang, Anti-freezing aqueous electrolytes for electric double-layer capacitors, Electrochim. Acta 88 (2013) 208–216, https://doi.org/10.1016/j.electacta.2012.10.047.
[149] Q. Abbas, F. Béguin, High voltage AC/AC electrochemical capacitor operating at low temperature in salt aqueous electrolyte, J. Power Sources 318 (2016) 235–241, https://doi.org/10.1016/j.jpowsour.2016.03.088.
[150] A.J. Roberts, A.F. Danil de Namor, R.C. Slade, Low temperature water based electrolytes for MnO2/carbon supercapacitors, Phys. Chem. Chem. Phys. 15 (10) (2013) 3518–3526, https://doi.org/10.1039/c3cp50359c.
[151] J. Menzel, E. Frackowiak, K. Fic, Electrochemical capacitor with water-based electrolyte operating at wide temperature range, J. Power Sources 414 (2019) 183–191, https://doi.org/10.1016/j.jpowsour.2018.12.080.
[152] S. Chen, C. Peng, D. Xue, L. Ma, C. Zhi, Alkaline tolerant antifreezing additive enabling aqueous Zn||Ni battery operating at -60 degrees C, Angew Chem. Int. Ed. Engl. 61 (48) (2022) e202212767, https://doi.org/10.1002/anie.202212767.
[153] S. Huang, S. He, Y. Li, S. Wang, X. Hou, Hydrogen bond acceptor lined hydrogel electrolyte toward Dendrite-Free aqueous Zn ion batteries with low temperature adaptability, Chem. Eng. J. 464 (2023), https://doi.org/10.1016/j.cej.2023.142607.
[154] D. Wu, W.Y. Zhang, H.J. Feng, Z.J. Zhang, X.Y. Chen, P. Cui, Mechanistic insights into the intermolecular interaction and Li+ solvation structure in small-molecule crowding electrolytes for high-voltage aqueous supercapacitors, ACS Appl. Energy Mater. 5 (10) (2022) 12067–12077, https://doi.org/10.1021/acsaem.2c01488.
[155] Q. Nian, J. Wang, S. Liu, T. Sun, S. Zheng, Y. Zhang, Z. Tao, J. Chen, Aqueous batteries operated at −50 °C, Angew. Chem. Int. Ed. 58 (47) (2019) 16994–16999, https://doi.org/10.1002/anie.201908913.
[156] Q. Nian, X. Zhang, Y. Feng, S. Liu, T. Sun, S. Zheng, X. Ren, Z. Tao, D. Zhang, J. Chen, Designing electrolyte structure to suppress hydrogen evolution reaction in aqueous batteries, ACS Energy Lett. 6 (6) (2021) 2174–2180, https://doi.org/10.1021/acsenergylett.1c00833.
[157] X. Lu, R.J. Jimenez-Rioboo, D. Leech, M.C. Gutierrez, M.L. Ferrer, F. Del Monte, Aqueous-Eutectic-in-Salt electrolytes for high-energy-density supercapacitors with an operational temperature window of 100 degrees C, from -35 to +65 degrees C, ACS Appl. Mater. Interfaces 12 (26) (2020) 29181–29193, https://doi.org/10.1021/acsami.0c04011.
[158] E. Perricone, M. Chamas, L. Cointeaux, J.C. Leprêtre, P. Judeinstein, P. Azais, F. Béguin, F. Alloin, Investigation of methoxypropionitrile as co-solvent for ethylene carbonate based electrolyte in supercapacitors. A safe and wide temperature range electrolyte, Electrochim. Acta 93 (2013) 1–7, https://doi.org/10.1016/j.electacta.2013.01.084.
[159] R.R. Galimzyanov, S.V. Stakhanova, I.S. Krechetov, A.T. Kalashnik, M.V. Astakhov, A.V. Lisitsin, A.Y. Rychagov, T.R. Galimzyanov, F.S. Tabarov, Electrolyte mixture based on acetonitrile and ethyl acetate for a wide temperature range performance of the supercapacitors, J. Power Sources 495 (2021), https://doi.org/10.1016/j.jpowsour.2020.229442.
[160] Y.-R. Tsai, B. Vedhanarayanan, T.-Y. Chen, Y.-C. Lin, J.-Y. Lin, X. Ji, T.-W. Lin, A tailor-made deep eutectic solvent for 2.2 V wide temperature-tolerant supercapacitors via optimization of N,N-dimethylformamide/water co-solvents, J. Power Sources 521 (2022), https://doi.org/10.1016/j.jpowsour.2021.230954.
[161] S. Li, Q. Tian, J. Chen, Y. Chen, P. Guo, C. Wei, P. Cui, J. Jiang, X. Li, Q. Xu, An intrinsically non-flammable organic electrolyte for wide temperature range supercapacitors, Chem. Eng. J. 457 (2023), https://doi.org/10.1016/j.cej.2022.141265.
[162] S.I. Wong, H. Lin, T. Ma, J. Sunarso, B.T. Wong, B. Jia, Binary ionic liquid electrolyte design for ultrahigh-energy density graphene-based supercapacitors, Materials Rep.: Energy 2 (2) (2022), https://doi.org/10.1016/j.matre.2022.100093.
[163] E.P. Yambou, B. Gorska, F. Béguin, Binary mixtures of ionic liquids based on EMIm cation and fluorinated anions: physico-chemical characterization in view of their application as low-temperature electrolytes, J. Mol. Liq. 298 (2020), https://doi.org/10.1016/j.molliq.2019.111959.
[164] O. Nordness, J.F. Brennecke, Ion dissociation in ionic liquids and ionic liquid solutions, Chem. Rev. 120 (23) (2020) 12873–12902, https://doi.org/10.1021/acs.chemrev.0c00373.
[165] Q. Zhang, K. De Oliveira Vigier, S. Royer, F. Jerome, Deep eutectic solvents: syntheses, properties and applications, Chem. Soc. Rev. 41 (21) (2012) 7108–7146, https://doi.org/10.1039/c2cs35178a.
[166] Y. Liu, J.B. Friesen, J.B. McAlpine, D.C. Lankin, S.N. Chen, G.F. Pauli, Natural deep eutectic solvents: properties, applications, and perspectives, J. Nat. Prod. 81 (3) (2018) 679–690, https://doi.org/10.1021/acs.jnatprod.7b00945.
[167] M. Zhong, Q.F. Tang, Y.W. Zhu, X.Y. Chen, Z.J. Zhang, An alternative electrolyte of deep eutectic solvent by choline chloride and ethylene glycol for wide temperature range supercapacitors, J. Power Sources 452 (2020), https://doi.org/10.1016/j.jpowsour.2020.227847.
[168] M. Zhong, Q.F. Tang, Z.G. Qiu, W.P. Wang, X.Y. Chen, Z.J. Zhang, A novel electrolyte of ternary deep eutectic solvent for wide temperature region supercapacitor with superior performance, J. Energy Storage 32 (2020), https://doi.org/10.1016/j.est.2020.101904.

[169] Z.-Y. Liu, Y. Liu, Y. Xu, H. Zhang, Z. Shao, Z. Wang, H. Chen, Novel high-entropy oxides for energy storage and conversion: from fundamentals to practical applications, Green Energy Environ. 8 (5) (2023) 1341–1357, https://doi.org/10.1016/j.gee.2023.04.007.
[170] M. Qiu, P. Sun, K. Han, Z. Pang, J. Du, J. Li, J. Chen, Z.L. Wang, W. Mai, Tailoring water structure with high-tetrahedral-entropy for antifreezing electrolytes and energy storage at −80 °C, Nat. Commun. 14 (1) (2023), https://doi.org/10.1038/s41467-023-36198-5.
[171] W. Zhang, H. Xia, Z. Zhu, Z. Lv, S. Cao, J. Wei, Y. Luo, Y. Xiao, L. Liu, X. Chen, Decimal solvent-based high-entropy electrolyte enabling the extended survival temperature of lithium-ion batteries to −130 °C, CCS Chem. 3 (4) (2021) 1245–1255, https://doi.org/10.31635/ccschem.020.202000341.
[172] S.C. Kim, J. Wang, R. Xu, P. Zhang, Y. Chen, Z. Huang, Y. Yang, Z. Yu, S.T. Oyakhire, W. Zhang, L.C. Greenburg, M.S. Kim, D.T. Boyle, P. Sayavong, Y. Ye, J. Qin, Z. Bao, Y. Cui, High-entropy electrolytes for practical lithium metal batteries, Nat. Energy 8 (8) (2023) 814–826, https://doi.org/10.1038/s41560-023-01280-1.
[173] H. Ji, C. Xie, T. Wu, H. Wang, Z. Cai, Q. Zhang, W. Li, L. Fu, H. Li, H. Wang, High-entropy solvent design enabling a universal electrolyte with a low freezing point for low-temperature aqueous batteries, Chem. Commun. 59 (56) (2023) 8715–8718, https://doi.org/10.1039/d3cc02214e.
[174] C. Yang, J. Xia, C. Cui, T.P. Pollard, J. Vatamanu, A. Faraone, J.A. Dura, M. Tyagi, A. Kattan, E. Thimsen, J. Xu, W. Song, E. Hu, X. Ji, S. Hou, X. Zhang, M.S. Ding, S. Hwang, D. Su, Y. Ren, X.-Q. Yang, H. Wang, O. Borodin, C. Wang, All-temperature zinc batteries with high-entropy aqueous electrolyte, Nat. Sustain. 6 (3) (2023) 325–335, https://doi.org/10.1038/s41893-022-01028-x.
[175] J. Tu, J. Pan, X. Liu, Y. Yan, Y. Shi, X. Yu, X. Jia, A flexible solid-state supercapacitor with extreme low-temperature tolerance based on an ion conducting ice gel electrolyte, J. Mater. Chem. A 10 (13) (2022) 7036–7047, https://doi.org/10.1039/d1ta08465h.
[176] X. Hou, Q. Zhang, L. Wang, G. Gao, W. Lu, Low-temperature-resistant flexible solid supercapacitors based on organohydrogel electrolytes and microvoid-incorporated reduced graphene oxide electrodes, ACS Appl. Mater. Interfaces 13 (10) (2021) 12432–12441, https://doi.org/10.1021/acsami.0c18741.
[177] T. Xu, D. Yang, S. Zhang, T. Zhao, M. Zhang, Z.-Z. Yu, Antifreezing and stretchable all-gel-state supercapacitor with enhanced capacitances established by graphene/PEDOT-polyvinyl alcohol hydrogel fibers with dual networks, Carbon 171 (2021) 201–210, https://doi.org/10.1016/j.carbon.2020.08.071.
[178] J. Xu, R. Jin, X. Ren, G. Gao, A wide temperature-tolerant hydrogel electrolyte mediated by phosphoric acid towards flexible supercapacitors, Chem. Eng. J. 413 (2021), https://doi.org/10.1016/j.cej.2020.127446.
[179] Q. Chen, L. Wang, J. Chen, Low-temperature and high-voltage-tolerant zinc-ion hybrid supercapacitor based on a hydrogel electrolyte, Chemelectrochem 9 (10) (2022), https://doi.org/10.1002/celc.202200070.
[180] D.K. Nandakumar, J.V. Vaghasiya, L. Suresh, T.N. Duong, S.C. Tan, Organic ionic conductors infused aqueous inverse-melting electrolyte aiding crack recovery in flexible supercapacitors functional down to −30 °C, Mater. Today Energy 17 (2020), https://doi.org/10.1016/j.mtener.2020.100428.
[181] T. Deng, W. Zhang, H. Zhang, W. Zheng, Anti-freezing aqueous electrolyte for high-performance Co(OH)2 supercapacitors at −30 °C, Energy Technol. 6 (4) (2018) 605–612, https://doi.org/10.1002/ente.201700648.
[182] H. Wang, J. Liu, J. Wang, M. Hu, Y. Feng, P. Wang, Y. Wang, N. Nie, J. Zhang, H. Chen, Q. Yuan, J. Wu, Y. Huang, Concentrated hydrogel electrolyte-enabled aqueous rechargeable NiCo//Zn battery working from −20 to 50 °C, ACS Appl. Mater. Interfaces 11 (1) (2019) 49–55, https://doi.org/10.1021/acsami.8b18003.
[183] Z. Wang, H. Li, Z. Tang, Z. Liu, Z. Ruan, L. Ma, Q. Yang, D. Wang, C. Zhi, Hydrogel electrolytes for flexible aqueous energy storage devices, Adv. Funct. Mater. 28 (48) (2018) 1804560, https://doi.org/10.1002/adfm.201804560.
[184] C. Zhong, Y. Deng, W. Hu, J. Qiao, L. Zhang, J. Zhang, A review of electrolyte materials and compositions for electrochemical supercapacitors, Chem. Soc. Rev. 44 (21) (2015) 7484–7539, https://doi.org/10.1039/c5cs00303b.
[185] C. Lu, X. Chen, All-temperature flexible supercapacitors enabled by antifreezing and thermally stable hydrogel electrolyte, Nano Lett. 20 (3) (2020) 1907–1914, https://doi.org/10.1021/acs.nanolett.9b05148.
[186] Y. Zhou, C. Wan, Y. Yang, H. Yang, S. Wang, Z. Dai, K. Ji, H. Jiang, X. Chen, Y. Long, Highly stretchable, elastic, and ionic conductive hydrogel for artificial soft electronics, Adv. Funct. Mater. 29 (1) (2019) 1806220, https://doi.org/10.1002/adfm.201806220.
[187] Y. Huang, M. Zhong, Y. Huang, M. Zhu, Z. Pei, Z. Wang, Q. Xue, X. Xie, C. Zhi, A self-healable and highly stretchable supercapacitor based on a dual crosslinked polyelectrolyte, Nat. Commun. 6 (1) (2015), https://doi.org/10.1038/ncomms10310.
[188] Z. Qin, X. Sun, H. Zhang, Q. Yu, X. Wang, S. He, F. Yao, J. Li, A transparent, ultrastretchable and fully recyclable gelatin organohydrogel based electronic sensor with broad operating temperature, J. Mater. Chem. A 8 (8) (2020) 4447–4456, https://doi.org/10.1039/c9ta13196e.
[189] Q. Rong, W. Lei, J. Huang, M. Liu, Low temperature tolerant organohydrogel electrolytes for flexible solid-state supercapacitors, Adv. Energy Mater. 8 (31) (2018), https://doi.org/10.1002/aenm.201801967.
[190] Y. Liu, H. Li, X. Wang, T. Lv, K. Dong, Z. Chen, Y. Yang, S. Cao, T. Chen, Flexible supercapacitors with high capacitance retention at temperatures from −20 to 100 °C based on DMSO-doped polymer hydrogel electrolytes, J. Mater. Chem. A 9 (20) (2021) 12051–12059, https://doi.org/10.1039/d1ta02397g.
[191] W. Wang, Y. Liu, S. Wang, X. Fu, T. Zhao, X. Chen, Z. Shao, Physically cross-linked silk fibroin-based tough hydrogel electrolyte with exceptional water retention and freezing tolerance, ACS Appl. Mater. Interfaces 12 (22) (2020) 25353–25362, https://doi.org/10.1021/acsami.0c07558.
[192] G. Zhang, S. Ge, T. Xu, X.-G. Yang, H. Tian, C.-Y. Wang, Rapid self-heating and internal temperature sensing of lithium-ion batteries at low temperatures, Electrochim. Acta 218 (2016) 149–155, https://doi.org/10.1016/j.electacta.2016.09.117.
[193] Y. Ji, C.Y. Wang, Heating strategies for Li-ion batteries operated from subzero temperatures, Electrochim. Acta 107 (2013) 664–674, https://doi.org/10.1016/j.electacta.2013.03.147.
[194] C.Y. Wang, G. Zhang, S. Ge, T. Xu, Y. Ji, X.G. Yang, Y. Leng, Lithium-ion battery structure that self-heats at low temperatures, Nature 529 (7587) (2016) 515–518, https://doi.org/10.1038/nature16502.
[195] Y. Sun, P. Ma, L. Liu, J. Chen, X. Zhang, J. Lang, X. Yan, Solar-thermal driven self-heating of micro-supercapacitors at low temperatures, Sol. RRL 2 (12) (2018), https://doi.org/10.1002/solr.201800223.
[196] P. Ma, Y. Sun, X. Zhang, J. Chen, B. Yang, Q. Zhang, X. Gao, X. Yan, Spinel-type solar-thermal conversion coatings on supercapacitors: an effective strategy for capacitance recovery at low temperatures, Energy Storage Mater. 23 (2019) 159–167, https://doi.org/10.1016/j.ensm.2019.05.016.
[197] S. Chen, L. Wang, X. Hu, Photothermal supercapacitors at −40 °C based on bifunctional TiN electrodes, Chem. Eng. J. 423 (2021), https://doi.org/10.1016/j.cej.2021.130162.
[198] X. Yu, N. Li, S. Zhang, C. Liu, L. Chen, M. Xi, Y. Song, S. Ali, O. Iqbal, M. Han, C. Jiang, Z. Wang, Enhancing the energy storage capacity of graphene supercapacitors via solar heating, J. Mater. Chem. A 10 (7) (2022) 3382–3392, https://doi.org/10.1039/d1ta09222g.